

Nature of the $X(5568)$: a critical Laplace sum rule analysis at N2LO

R. Albuquerque

Faculty of Technology, Rio de Janeiro State University (FAT, UERJ), Brazil

Email address: raphael.albuquerque@uerj.br

S. Narison*

*Laboratoire Univers et Particules de Montpellier, CNRS-IN2P3,
Case 070, Place Eugène Bataillon, 34095 - Montpellier, France.*

Email address: snarison@yahoo.fr

A. Rabemananjara and D. Rabetiarivony

Institut of High-Energy Physics of Madagascar (iHEPMAD)

University of Ambohitsaina, Antananarivo 101, Madagascar

We scrutinize recent QCD spectral sum rules (QSSR) results to lowest order (LO) predicting the masses of the BK molecule and $(su)(\bar{b}\bar{d})$ four-quark states. We improve these results by adding NLO and N2LO corrections to the PT contributions giving a more precise meaning on the b -quark mass definition used in the analysis. We extract our optimal predictions using Laplace sum rule (LSR) within the *standard stability criteria* versus the changes of the external free parameters (τ -sum rule variable, t_c continuum threshold and subtraction constant μ). The smallness of the higher order PT corrections justifies (a posteriori) the LO order results \oplus the uses of the ambiguous heavy quark mass to that order. However, our predicted spectra in the range (5173 \sim 5226) MeV, summarized in Table 7, for exotic hadrons built with four different flavours ($buds$), do not support some previous interpretations of the $D0$ candidate,¹ $X(5568)$, as a pure molecule or a four-quark state. If experimentally confirmed, it could result from their mixing with an angle: $\sin 2\theta \approx 0.15$. One can also scan the region (2327 \sim 2444) MeV (where the $D_{s0}^*(2317)$ might be a good candidate) and the one (5173 \sim 5226) MeV for detecting these ($cuds$) and ($buds$) unmixed exotic hadrons (if any) via, eventually, their radiative or $\pi + hadrons$ decays.

Keywords: QCD spectral sum rules, Perturbative and Non-perturbative calculations, Exotic Hadrons, Hadron Masses, Leptonic decays.

Pac numbers: 11.55.Hx, 12.38.Lg, 13.20-v

*In writing this paper, I learn the sudden death of my collaborator and friend Gerard Mennessier. I dedicate my contribution in this paper for his memory.

2 *R.M. Albuquerque et al.*

1. Introduction and Experimental Facts

Stimulated by the recent observation of the $D0$ collaboration for a narrow $X(5568)$ state ($\Gamma_X = 21.9 \pm 6.4_{-2.5}^{+5.0}$ MeV) decaying sequentially into $B_s^0 \pi^\pm$: $B_s^0 \rightarrow J/\psi \phi$, $J/\psi \rightarrow \mu^+ \mu^-$, $\phi \rightarrow K^+ K^-$, where a $J^P = 0^+$ is favoured, many papers have been proposed in the literature for explaining its nature. If confirmed^a, this is the first observation of an hadron bounded with four-different flavours (*buds*) which cannot be accomodated by the usual quark model but instead by a four-quark or a molecule or some other exotic mechanism. Among different proposals, we select the ones from QCD spectral sum rules (QSSR)^{3,4}^b, which interpret the $X(5568)$ state either as a BK molecule¹⁴ or as a four-quark $(\bar{b}u)(ds)^{15-18}$ exotic bound state.

2. Interpolating currents

• In the following, we shall analyze different assumptions on the nature of the $X(5568)$ which can be specified by the form of the minimal QCD interpolating currents given in Table 1. C is the charge conjugation matrix; u, d, s, b are the

Table 1. Minimal interpolating currents J_X describing the $X(5568)$

Nature	J^P	Current
<i>Molecule</i>		
BK	0^+	$(\bar{b} i \gamma_5 u)(\bar{d} i \gamma_5 s)$
$B_s \pi$	0^+	$(\bar{b} i \gamma_5 s)(\bar{d} i \gamma_5 u)$
$B^* K$	1^+	$(\bar{b} i \gamma_\mu u)(\bar{d} i \gamma_5 s)$
$B_s^* \pi$	1^+	$(\bar{b} i \gamma_\mu s)(\bar{d} i \gamma_5 u)$
<i>Four-quark</i>		
	1^-	$(s^T C \gamma_5 u)(\bar{b} \gamma_\mu \gamma_5 C \bar{d}^T) + k(s^T C u)(\bar{b} \gamma_\mu C \bar{d}^T)$
	1^+	$(s^T C \gamma_5 u)(\bar{b} \gamma_\mu C \bar{d}^T) + k(s^T C u)(\bar{b} \gamma_\mu \gamma_5 C \bar{d}^T)$

quark fields and the summation over colour indices is understood; k is a free mixing parameter.

- The corresponding scalar two-point correlator is defined as:

$$\psi_X(q^2) = i \int d^4x e^{-iqx} \langle 0 | J_X(x) J_X^\dagger(0) | 0 \rangle, \quad (1)$$

The vector or axial-vector correlator reads:

$$\begin{aligned} \Pi_X^{\mu\nu}(q^2) &= i \int d^4x e^{-iqx} \langle 0 | J_X^\mu(x) (J_X^\nu(0))^\dagger | 0 \rangle \\ &\equiv - \left(g^{\mu\nu} - \frac{q^\mu q^\nu}{q^2} \right) \Pi_X^{(1)}(q^2) + \frac{q^\mu q^\nu}{q^2} \Pi_X^{(0)}(q^2), \end{aligned} \quad (2)$$

^aNote that a recent analysis of the LHCb collaboration does not confirm this $D0$ result.²

^bFor reviews where complete references can be found, see e.g.⁵⁻¹³

where the longitudinal part : $\Pi_X^{(0)}(q^2)$ is related to the (pseudo)scalar correlator $\psi_X(q^2)$ via a well-known Ward identity. We shall be concerned here with the transverse part $\Pi_X^{(1)}(q^2)$ which has the quantum number : $J^P = 1^+$ or 1^- and its longitudinal part: $\Pi_X^{(0)}(q^2)$ with the quantum number: $J^P = 0^+$ or 0^- .

- The previous correlators obey the Källén-Lehmann representation or dispersion relation:

$$\Pi_X(q^2) = \int_{(M_b+m_s)^2}^{\infty} \frac{dt}{t - q^2 - i\epsilon} \frac{1}{\pi} \text{Im}\Pi_X(t) + \dots, \quad (3)$$

where \dots represents subtraction constants which are polynomial in q^2 ; $\Pi_X \equiv \psi_X$ or $\Pi_X^{(0,1)}$; $(1/\pi)\text{Im}\Pi_X(t) \equiv \rho(t)$ is the spectral function that can be measured experimentally or calculable in QCD for large values of t .

3. The inverse Laplace transform sum rule (LSR)

- One can improve the previous Källén-Lehmann representation by applying to both sides n -numbers of derivative in $Q^2 \equiv -q^2$ and by keeping the ratio $n/Q^2 \equiv \tau$ fixed. In this way, it becomes an exponential sum rule:

$$\mathcal{L}(\tau, \mu) \equiv \int_{(M_b+m_s)^2}^{\infty} dt e^{-t\tau} \rho(t, \mu), \quad (4)$$

$$\mathcal{R}(\tau, \mu) = \frac{\int_{(M_b+m_s)^2}^{\infty} dt t e^{-t\tau} \rho(t, \mu)}{\int_{(M_b+m_s)^2}^{\infty} dt e^{-t\tau} \rho(t, \mu)}, \quad (5)$$

where μ is the subtraction point which appears in the approximate QCD series when radiative corrections are included. The set of variables (τ, μ) are, in principle, free external parameters. We shall use stability criteria (if any) for extracting the optimal results.

- These sum rules firstly derived by SVZ^{3,4} have been called Borel sum rule due to the factorial suppression factor of the condensate contributions in the OPE. Their quantum mechanics version have been studied by Bell-Bertlmann in^{19,20} through the harmonic oscillator where τ has the property of an imaginary time, while the derivation of their radiative corrections has been firstly shown by Narison-de Rafael²¹ to have the properties of the inverse Laplace sum rule (LSR).

4. Parametrization of the spectral function and Stability criteria

- The ratio^{3,4,19,20} and double ratio^{22 c} of sum rules :

$$\mathcal{R}_{S/A}(\tau, \nu) \quad \text{and} \quad \mathcal{R}_{A,S}(\tau, \nu) \equiv \frac{\mathcal{R}_A}{\mathcal{R}_S}, \quad (6)$$

^cThe double ratio of sum rules have been successfully applied in different channels.²⁴⁻³³

4 *R.M. Albuquerque et al.*

are useful, as they are equal to the resonance mass squared $M_{S/A}^2$ and their ratio at the τ -stability region:

$$\mathcal{R}_{S/A} \simeq M_{S/A}^2 \quad \text{and} \quad \mathcal{R}_{A,S} \simeq \frac{M_A^2}{M_S^2}, \quad (7)$$

in the Minimal Duality Ansatz (MDA) parametrization of the spectral function:

$$\rho_{S/A}(t) \simeq f_{S/A}^2 M_{S/A}^8 \delta(t - M_{S/A}^2) + \text{“QCD continuum”} \theta(t - t_c), \quad (8)$$

where $f_{S/A}$ is the leptonic decay constant or coupling defined as:

$$\langle 0 | J_S | S \rangle = f_S M_S^4 \quad \text{and} \quad \langle 0 | J_A^\mu | A \rangle = \epsilon^\mu f_A M_A^5, \quad (9)$$

respectively for the scalar (S) and axial-vector (A) mesons, where ϵ^μ is the W -boson polarization, while the “QCD continuum” comes from the discontinuity of the Feynmann diagrams appearing in the SVZ expansion. Though apparently quite simple, different tests of this MDA from complete hadronic data have shown that it can reproduce with high-precision these complete data,^{7,8,34,35} while it has been also successfully tested in the large N_c limit of QCD.^{36,37}

• Noting that in the previous definition in Table 1, the bilinear pseudoscalar current acquires an anomalous dimension due to its normalization, thus the X -decay constant runs for $n_f = 5$ and to α_s^2 as :

$$f_S(\mu) = \hat{f}_S (-\beta_1 a_s)^{4/\beta_1} / r_m^2, \quad f_A(\mu) = \hat{f}_A (-\beta_1 a_s)^{2/\beta_1} / r_m \quad (10)$$

where we have introduced the renormalization group invariant coupling $\hat{f}_{S/A}$; $-\beta_1 = (1/2)(11 - 2n_f/3)$ is the first coefficient of the QCD β -function for n_f flavours and $a_s \equiv (\alpha_s/\pi)$. For $n_f = 5$ flavours, the QCD corrections read;

$$r_m = 1 + 1.176 \left(\frac{\alpha_s}{\pi} \right) + 1.501 \left(\frac{\alpha_s}{\pi} \right)^2. \quad (11)$$

• Optimal information on the lowest resonance mass and decay constant can be achieved at the stability regions (if they exist) of the set of external variables (τ, t_c, μ) . This requirement is similar to the Principle of Minimal Sensitivity (PMS) used, e.g, in³⁸ for optimized perturbative series.

5. QCD expressions of the B^*K and BK spectral functions

We give below the QCD expressions of the B^*K and BK two-point spectral function at lowest order (LO) of perturbation theory and including the quark and gluon condensates within the SVZ operator product expansion (OPE). The value and normalization of these condensates are given in Table 2 and in Section 6.

5.1. $B^*K (1^+)$ axial-vector molecule

For the axial-vector 1^+ molecule, the spectral function reads up to dimension 6 condensates:

$$\begin{aligned}
\rho^{pert} &= \frac{M_b^8}{5 \cdot 3 \cdot 2^{15} \pi^6} \left[\frac{5}{x^4} - \frac{96}{x^3} - \frac{945}{x^2} + \frac{480}{x} - 60 \left(\frac{9}{x^2} + \frac{16}{x} + 3 \right) \text{Log } x + 555 + x^2 \right], \\
\rho^{\langle \bar{q}q \rangle} &= -\frac{M_b^5}{2^8 \pi^4} \langle \bar{q}q \rangle \left[\frac{1}{x^2} + \frac{9}{x} + 6 \left(\frac{1}{x} + 1 \right) \text{Log } x - 9 - x \right] - \\
&\quad \frac{m_s M_b^4}{2^{11} \pi^4} \langle \bar{q}q \rangle (2 - \kappa) \left(\frac{3}{x^2} - \frac{16}{x} - 12 \text{Log } x + 12 + x^2 \right), \\
\rho^{\langle G^2 \rangle} &= \frac{M_b^4}{3 \cdot 2^{15} \pi^6} 4\pi \langle \alpha_s G^2 \rangle \left[\frac{1}{x^2} - \frac{120}{x} - 12 \left(\frac{4}{x} + 7 \right) \text{Log } x + 108 + 8x + 3x^2 \right], \\
\rho^{\langle \bar{q}Gq \rangle} &= \frac{3M_b^3}{2^9 \pi^4} \langle \bar{q}Gq \rangle \left(\frac{1}{x} + 2 \text{Log } x - x \right) + \frac{m_s M_b^2}{3 \cdot 2^9 \pi^4} \langle \bar{q}Gq \rangle (3 + 2\kappa) \left(\frac{2}{x} - 3 + x^2 \right), \\
\rho^{\langle \bar{q}q \rangle^2} &= \frac{M_b^2}{3 \cdot 2^5 \pi^2} \rho^{\langle \bar{q}q \rangle}^2 \kappa \left(\frac{2}{x} - 3 + x^2 \right) + \frac{m_s M_b}{2^5 \pi^2} \rho^{\langle \bar{q}q \rangle}^2 (2 - \kappa) (1 - x), \\
\rho^{\langle G^3 \rangle} &= \frac{M_b^2}{3^2 \cdot 2^{17} \pi^6} \langle g^3 G^3 \rangle \left[\frac{9}{x^2} - \frac{160}{x} - 12 \left(\frac{4}{x} + 9 \right) \text{Log } x + 144 + 7x^2 \right]. \tag{12}
\end{aligned}$$

where $: x = M_b^2/t$, and $\kappa \equiv \langle \bar{s}s \rangle / \langle \bar{q}q \rangle \simeq \langle \bar{s}Gs \rangle / \langle \bar{q}Gq \rangle$ measures the $SU(3)$ breaking of the quark and mixed quark condensates. The contribution of a class of $d = 7$ condensate for $m_s = 0$ is:

$$\rho^{\langle \bar{q}q \rangle \langle G^2 \rangle} = -\frac{M_b \langle \bar{q}q \rangle}{3 \cdot 2^9 \pi^4} 4\pi \langle \alpha_s G^2 \rangle \left(\frac{1}{x} + 3 \text{Log } x + 5 - 6x \right). \tag{13}$$

The previous expressions compared to the ones in the literature are more convenient to use as they are in an integrated form. One should note that:

- In performing the calculation of the spectral function, the heavy quark is put on-shell which corresponds to the implicit use of the pole mass M_b in the previous QCD expression. This feature does not justify the (a priori) use of the running mass in the sum rule analysis as done in the existing literature. We shall come back to this point later on.

- In the literature, dimension condensates larger than $d = 6$ have been also included in the OPE in order to improve stability of the results. However, one should note that the included condensates are only a part of more general condensates contributions at a given dimension. There is also a poor quantitative control of these high dimension condensates as has been hotly discussed in the past (cases of charmonium and ρ meson channels)^{7,8} due to the violation of factorization which is already about a factor 3-4 for the $d = 6$ condensates. This feature indicates that the error quoted in the final result which does not take into account such a violation has been largely underestimated. Therefore, we refrain to include these terms in the analysis but only consider them as a source of errors.

6 *R.M. Albuquerque et al.*

- We have not included in the OPE the $d = 2$ tachyonic gluon mass^{39,40 d} as it has been shown to be dual to the higher order terms of the PT series⁴³ which we shall estimate using a geometric growth of the PT coefficients.

5.2. $BK (0^+)$ scalar molecule

It reads up to the dimension 6 condensates:

$$\begin{aligned}
 \rho^{pert} &= \frac{M_b^8}{5 \cdot 2^{14} \pi^6} \left[\frac{1}{x^4} - \frac{20}{x^3} - \frac{220}{x^2} + \frac{80}{x} - 60 \left(\frac{2}{x^2} + \frac{4}{x} + 1 \right) \text{Log } x + 155 + 4x \right], \\
 \rho^{\langle \bar{q}q \rangle} &= -\frac{M_b^5}{2^8 \pi^4} \langle \bar{q}q \rangle \left[\frac{1}{x^2} + \frac{9}{x} + 6 \left(\frac{1}{x} + 1 \right) \text{Log } x - 9 - x \right] - \\
 &\quad \frac{m_s M_b^4}{2^9 \pi^4} \langle \bar{q}q \rangle (2 - \kappa) \left(\frac{1}{x^2} - \frac{6}{x} - 6 \text{Log } x + 3 + 2x \right), \\
 \rho^{\langle G^2 \rangle} &= \frac{M_b^4}{3 \cdot 2^{13} \pi^6} 4\pi \langle \alpha_s G^2 \rangle \left[\frac{5}{x^2} + 6 \left(\frac{2}{x} - 1 \right) \text{Log } x - 9 + 4x \right], \\
 \rho^{\langle \bar{q}Gq \rangle} &= \frac{3M_b^3}{2^8 \pi^4} \langle \bar{q}Gq \rangle \left[\frac{3}{x} + \left(\frac{1}{x} + 3 \right) \text{Log } x - 2 - x \right] + \\
 &\quad \frac{m_s M_b^2}{2^9 \pi^4} \langle \bar{q}Gq \rangle (3 + 2\kappa) \left(\frac{1}{x} - 2 + x \right), \\
 \rho^{\langle \bar{q}q \rangle^2} &= \frac{M_b^2}{2^5 \pi^2} \rho^{\langle \bar{q}q \rangle^2} \kappa \left(\frac{1}{x} - 2 + x \right) + \frac{m_s M_b}{2^5 \pi^2} \rho^{\langle \bar{q}q \rangle^2} (2 - \kappa) (1 - x), \\
 \rho^{\langle G^3 \rangle} &= \frac{M_b^2}{3 \cdot 2^{15} \pi^6} \langle g^3 G^3 \rangle \left[\frac{1}{x^2} - \frac{21}{x} - 6 \left(\frac{1}{x} + 3 \right) \text{Log } x + 15 + 5x \right]. \tag{14}
 \end{aligned}$$

The contribution of a class of $d = 7$ condensate for $m_s = 0$ is:

$$\rho^{\langle \bar{q}q \rangle \langle G^2 \rangle} = -\frac{M_b \langle \bar{q}q \rangle}{3 \cdot 2^9 \pi^4} 4\pi \langle \alpha_s G^2 \rangle \left(\frac{1}{x} + 12 \text{Log } x + 14 - 15x \right). \tag{15}$$

5.3. Higher Order (HO) PT corrections to the Spectral function

- We extract the Higher Order (HO) PT corrections by considering that the molecule two-point spectral function is the convolution of the two ones built from two quark bilinear currents (factorization) as a consequence of the molecule defini-

^dFor reviews, see e.g.^{41,42}

tion of the state^e:

$$\begin{aligned}
J_K(x) &\equiv \bar{d}i\gamma_5 s \quad \rightsquigarrow \quad \frac{1}{\pi} \text{Im}\psi_K(t) , \\
J_B(x) &\equiv \bar{b}i\gamma_5 u \quad \rightsquigarrow \quad \frac{1}{\pi} \text{Im}\psi_B(t) , \\
J_{B^*}^\mu(x) &\equiv \bar{b}\gamma^\mu u \quad \rightsquigarrow \quad \frac{1}{\pi} \text{Im}\Pi_{B^*}(t) .
\end{aligned} \tag{16}$$

In this way, we obtain the convolution integral for the axial-vector state⁴⁶ :

$$\begin{aligned}
\frac{1}{\pi} \text{Im}\Pi_A(t) &= \theta(t - (M_b + m_s)^2) \left(\frac{1}{4\pi} \right)^2 t^2 \int_{M_b^2}^{(\sqrt{t}-m_s)^2} dt_1 \int_{m_s^2}^{(\sqrt{t}-\sqrt{t_1})^2} dt_2 \lambda^{3/2} \\
&\times \frac{1}{\pi} \text{Im}\Pi_{B^*}(t_1) \frac{1}{\pi} \text{Im}\psi_K(t_2),
\end{aligned} \tag{17}$$

and for the scalar state^{46,47} :

$$\begin{aligned}
\frac{1}{\pi} \text{Im}\psi_S(t) &= \theta(t - (M_b + m_s)^2) \left(\frac{1}{4\pi} \right)^2 t^2 \int_{M_b^2}^{(\sqrt{t}-m_s)^2} dt_1 \int_{m_s^2}^{(\sqrt{t}-\sqrt{t_1})^2} dt_2 \lambda^{1/2} \\
&\times \left(\frac{t_1}{t} + \frac{t_2}{t} - 1 \right)^2 \times \frac{1}{\pi} \text{Im}\psi_B(t_1) \frac{1}{\pi} \text{Im}\psi_K(t_2),
\end{aligned} \tag{18}$$

with the phase space factor :

$$\lambda = \left(1 - \frac{(\sqrt{t_1} - \sqrt{t_2})^2}{t} \right) \left(1 - \frac{(\sqrt{t_1} + \sqrt{t_2})^2}{t} \right) . \tag{19}$$

M_b is the on-shell(pole) perturbative heavy quark mass, while we shall use the running perturbative mass \bar{m}_s in the \overline{MS} -scheme.

- The perturbative expressions of the bilinear unequal masses pseudoscalar $\text{Im}\psi_{K/B}(t)$ and $\text{Im}\Pi_{B^*}(t)$ spectral functions are known in the literature up to N2LO corrections.^{7,8} The complete LO expression has been evaluated firstly in,⁴⁸ the NLO corrections for light quarks by,⁴⁹ the complete NLO by⁵⁰ and the N2LO with one massless quark by.⁵¹

5.4. Relation between the pole and running heavy quark masses

- The PT expression of the spectral function obtained using on-shell renormalization can be transformed into the \overline{MS} -scheme by using the relation between the

^eA such approach has been used in^{44,45} for estimating *for the first time* the higher order perturbative corrections to the spectral functions of molecule states.

8 *R.M. Albuquerque et al.*

\overline{MS} running mass $\overline{m}_Q(\mu)$ and the on-shell mass M_Q , to order $\alpha_s^{2,52-61}$

$$M_Q = \overline{m}_Q(\mu) \left[1 + \frac{4}{3} a_s + (16.2163 - 1.0414 n_l) a_s^2 + \ln \left(\frac{\mu}{M_Q} \right)^2 (a_s + (8.8472 - 0.3611 n_l) a_s^2) + \ln^2 \left(\frac{\mu}{M_Q} \right)^2 (1.7917 - 0.0833 n_l) a_s^2 \dots \right], \quad (20)$$

for n_l light flavours.

6. QCD input parameters

Table 2. QCD input parameters: the original errors for $\langle \alpha_s G^2 \rangle$, $\langle g^3 G^3 \rangle$ and $\rho \langle \bar{q}q \rangle^2$ have been multiplied by about a factor 3 for a conservative estimate of the errors (see also the text).

Parameters	Values	Ref.
$\alpha_s(M_\tau)$	0.325(8)	62–66
$\overline{m}_c(m_c)$	1261(12) MeV	average ^{66–71}
$\overline{m}_b(m_b)$	4177(11) MeV	average ^{66–69}
$\hat{\mu}_q$	(253 ± 6) MeV	7, 27, 29, 72–74
\hat{m}_s	(0.114 ± 0.006) GeV	7, 27, 29, 72–74
$\kappa \equiv \langle \bar{s}s \rangle / \langle \bar{d}d \rangle$	$(0.74^{+0.34}_{-0.12})$	7, 31, 32
M_0^2	(0.8 ± 0.2) GeV ²	28, 75–80
$\langle \alpha_s G^2 \rangle$	$(7 \pm 3) \times 10^{-2}$ GeV ⁴	19, 20, 62, 67–69, 81–88
$\langle g^3 G^3 \rangle$	(8.2 ± 2.0) GeV ² $\times \langle \alpha_s G^2 \rangle$	67–69
$\rho \alpha_s \langle \bar{q}q \rangle^2$	$(5.8 \pm 1.8) \times 10^{-4}$ GeV ⁶	62, 75–77, 81

• The QCD parameters which shall appear in the following analysis will be the charm and bottom quark masses $m_{c,b}$ (we shall neglect the light quark masses $q \equiv u, d$), the light quark condensate $\langle \bar{q}q \rangle$, the gluon condensates $\langle \alpha_s G^2 \rangle \equiv \langle \alpha_s G_{\mu\nu}^a G_{\mu\nu}^{a\mu\nu} \rangle$ and $\langle g^3 G^3 \rangle \equiv \langle g^3 f_{abc} G_{\mu\nu}^a G_{\nu\rho}^b G_{\rho\mu}^c \rangle$, the mixed condensate $\langle \bar{q}Gq \rangle \equiv \langle \bar{q} g \sigma^{\mu\nu} (\lambda_a/2) G_{\mu\nu}^a q \rangle = M_0^2 \langle \bar{q}q \rangle$ and the four-quark condensate $\rho \alpha_s \langle \bar{q}q \rangle^2$, where $\rho \simeq 3 - 4$ indicates the deviation from the four-quark vacuum saturation. Their values are given in Table 2.

• We shall work with the running light quark condensates and masses. They read:

$$\langle \bar{q}q \rangle(\tau) = -\hat{\mu}_q^3 (-\beta_1 a_s)^{2/\beta_1}, \quad \langle \bar{q}Gq \rangle(\tau) = -M_0^2 \hat{\mu}_q^3 (-\beta_1 a_s)^{1/3\beta_1}, \quad (21)$$

$\hat{\mu}_q$ is the spontaneous RGI light quark condensate.⁴⁸ We shall use:

$$\alpha_s(M_\tau) = 0.325(8) \rightsquigarrow \alpha_s(M_Z) = 0.1192(10) \quad (22)$$

Table 3. $\alpha_s(\mu)$ and correlated values of the running mass $\bar{m}_Q(\mu)$ used in the analysis for different values of the subtraction scale μ . The error in $\bar{m}_Q(\mu)$ has been induced by the one of $\alpha_s(\mu)$ to which one has added the error on their determination given in Table 2.

Input for $BK, B^*K, (b\bar{u})(ds): n_f = 5$		
$\mu[\text{GeV}]$	$\alpha_s(\mu)$	$\bar{m}_b(\mu)[\text{GeV}]$
3	0.2590(26)	4.474(4)
3.5	0.2460(20)	4.328(2)
Input: $\bar{m}_b(m_b)$	0.2320(20)	4.177
4.5	0.2267(20)	4.119(1)
5.0	0.2197(18)	4.040(1)
5.5	0.2137(17)	3.973(2)
6.0	0.2085(16)	3.914(2)
6.5	0.2040(15)	3.862(2)
7.0	0.2000(15)	3.816(3)
Input for $DK, D^*K, (c\bar{u})(ds): n_f = 4$		
$\mu[\text{GeV}]$	$\alpha_s(\mu)$	$\bar{m}_c(\mu)[\text{GeV}]$
Input: $\bar{m}_c(m_c)$	0.4084(144)	1.26
1.5	0.3649(110)	1.176(5)
2	0.3120(77)	1.069(9)
2.5	0.2812(61)	1.005(10)
3.0	0.2606(51)	0.961(10)
3.5	0.2455(45)	0.929(11)
4.0	0.2339(41)	0.903(11)
4.5	0.2246(37)	0.882(11)
5.0	0.2169(35)	0.865(11)
5.5	0.2104(33)	0.851(12)
6.0	0.2049(30)	0.838(12)

from τ -decays^{62–64} (see also: ^{89–92}), which agree perfectly with the world average 2014:^{65,66}

$$\alpha_s(M_Z) = 0.1184(7) . \quad (23)$$

The value of the running $\langle \bar{q}q \rangle$ condensate is deduced from the well-known GMOR relation:

$$(m_u + m_d)\langle \bar{u}u + \bar{d}d \rangle = -m_\pi^2 f_\pi^2 , \quad (24)$$

where $f_\pi = 130.4(2)$ MeV⁹³ and the value of $(\bar{m}_u + \bar{m}_d)(2) = (7.9 \pm 0.6)$ MeV obtained in^{27,29} which agrees with the PDG in⁶⁶ and lattice averages in.⁹⁴ Then, we deduce the RGI light quark spontaneous mass $\hat{\mu}_q$ given in Table 2.

- For the heavy quarks, we shall use the running mass and the corresponding value of α_s evaluated at the scale μ . These sets of correlated parameters are given in Table 3 for different values of μ and for a given number of flavours n_f .

- For the $\langle \alpha_s G^2 \rangle$ condensate, we have enlarged the original error by a factor about 3 in order to have a conservative result and to recover the original SVZ

estimate and the alternative extraction in ^{70,71} from charmonium sum rules which we consider as the most reliable channel for extracting phenomenologically this condensate. However, a direct comparison of this range of values obtained within short QCD series (few terms) with the one from lattice calculations⁹⁵ obtained within a long QCD series remains to be clarified.⁹⁶

• Some other estimates of the gluon and four-quark condensates using τ -decay and $e^+e^- \rightarrow I = 1$ hadrons data can be found in ^{?,90–92,97,98} Due to the large uncertainties induced by the different resummations of the QCD series and by the less-controlled effects of some eventual duality violation, we do not consider explicitly these values in the following analysis. However, we shall see later on that the effects of the gluon and four-quark condensates on the values of the decay constants and masses are quite small though they play an important role in the stability analysis.

7. Mass and coupling of the B^*K (1^+) axial-vector molecule

7.1. τ - and t_c -stability criteria at lowest order (LO)

• We show in Fig.1 the τ - and t_c -behaviours of the mass and coupling of the B^*K axial-vector molecule at lowest order (LO) of perturbative QCD. We have used the running $\bar{m}_b(\mu)$ b -quark mass (though not a priori justified), while the OPE is truncated at $d = 6$.

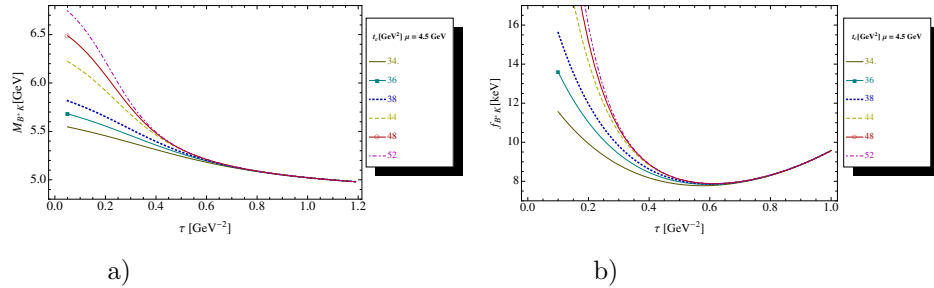


Fig. 1. **a)** M_{B^*K} at LO as function of τ for different values of t_c , $\mu = 4.5$ GeV and for the QCD parameters in Table 2 and 3; **b)** The same as a) but for the coupling f_{B^*K} .

• One can notice that the stabilities of both curves are reached for $\tau \simeq (0.45-0.5)$ GeV^{-2} . However, an important difference appears here : the coupling is dominated by the $d \leq 6$ non-perturbative condensates (minimum in τ) while the mass is dominated by the perturbative one at the inflexion point. This feature indicates already the exotic nature of this molecule state compared to ordinary heavy-light B -meson.^{5–8,34,35,99,100}

• We consider as an optimal value from the analysis, the one where the τ -stability about 0.6 GeV^{-2} starts for $t_c \geq 34 \text{ GeV}^2$, while the minimum sensitivity on the change of the continuum threshold t_c is reached for $t_c \simeq (44 - 48) \text{ GeV}^2$. Using

$\bar{m}_b(m_b)$ in Table 2, we consider as a conservative optimal value the results inside the above range:

$$M_{B^*K}^{LO} \simeq (5.19 \sim 5.20) \text{ GeV} \quad \text{and} \quad f_{B^*K}^{LO} \simeq (7.77 \sim 7.88) \text{ keV} \quad (25)$$

• Often added in the literature are the contributions of higher dimension condensates $d \geq 7$ for restoring the τ -stability of the sum rules. However, this procedure is not very helpful as the contribution of included high-dimension condensates come only from one class of diagrams generated by the quark propagator put in an external gluon fields. Moreover, these high-dimension condensates are poorly controlled due to the violation of factorization which already at $d = 6$ is expected to be violated by a factor 3-4 (see Table 2). Therefore, we conclude that predictions strongly depending on these high-dimension condensates are not reliable^f.

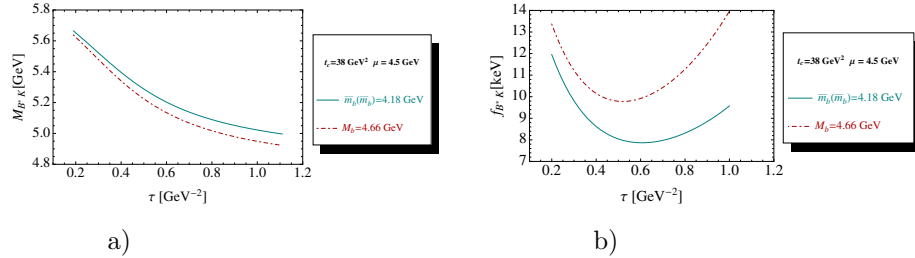


Fig. 2. **a)** M_{B^*K} at LO as function of τ for a given value of $t_c = 38 \text{ GeV}^2$, $\mu = 4.5 \text{ GeV}$ and for the QCD parameters in Tables 2 and 3. The OPE is truncated at $d = 6$ and the PT is at lowest order. We use the on-shell or pole mass $M_b = 4.66 \text{ GeV}$ and the running mass $\bar{m}_b(\bar{m}_b) = 4.18 \text{ GeV}$; **b)** The same as a) but for the coupling f_{B^*K} .

7.2. b -quark mass ambiguity at lowest order (LO)

Often used in the existing literature is the value of the running heavy quark mass $\bar{m}_b(m_b)$ into the expression of the spectral function evaluated at lowest order (LO) of perturbation theory (PT). Though, one should go beyond LO to see the clear selection among the two mass definitions, this is certainly misleading as the spectral function has been evaluated on-shell such that the mass to be used should be the on-shell or pole quark mass. We show in Fig. 2 the comparison of the result when we use the b -quark pole mass value of 4.66 GeV ⁶⁶ and the running mass $\bar{m}_b(m_b) = 4.18 \text{ GeV}$ in Table 2. This choice introduces an intrinsic source of error:

$$\Delta M_{B^*K}^{LO} \simeq 80 \text{ MeV} \quad \text{and} \quad \Delta f_{B^*K}^{LO} \simeq 2 \text{ keV} , \quad (26)$$

which is never considered in the existing literature.

^fWe shall explicitly check in the case of scalar molecule, which presents the same feature, that the $d = 7$ condensates contributions in Eq. 15 are negligible allowing a violation of factorization by a factor 4.

7.3. Higher order perturbative QCD corrections

For a more reliable prediction, one should improve the previous LO estimate. In so doing, we use the fact that the molecule spectral function is the convolution of the one of two-quark bilinear currents (factorization) which is a consequence of the molecule state definition. In the case of the B^*K molecule, this corresponds to the convolution of the B^* and K mesons spectral functions. The convolution expression is given in Eq. 17.

- We show the results including the NLO perturbative corrections in Fig. 3 versus τ for three values of t_c . The inclusion of the NLO corrections modify the previous

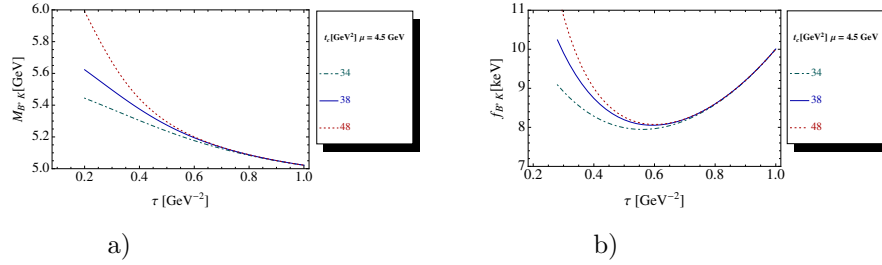


Fig. 3. **a)** M_{B^*K} at NLO as function of τ for different values of t_c , $\mu = 4.5$ GeV and for the QCD parameters in Tables 2 and 3; **b)** The same as a) but for the coupling f_{B^*K} .

LO results for $t_c = (34 \sim 48) \text{ GeV}^2$ and $\tau \simeq (0.56 \sim 0.60) \text{ GeV}^{-2}$ to:

$$M_{B^*K}^{NLO} \simeq (5200 \sim 5201) \text{ MeV} \quad \text{and} \quad f_{B^*K}^{NLO} \simeq (7.95 \sim 8.07) \text{ keV}. \quad (27)$$

- In the same way as in previous analysis, we show the results including the N2LO perturbative corrections in Fig. 4 versus τ for three values of t_c . For $t_c = (34 \sim 48) \text{ GeV}^2$ and $\tau \simeq (0.58 \sim 0.62) \text{ GeV}^{-2}$, we obtain:

$$M_{B^*K}^{N2LO} \simeq (5185 \sim 5187) \text{ MeV} \quad \text{and} \quad f_{B^*K}^{N2LO} \simeq (7.95 \sim 8.09) \text{ keV}. \quad (28)$$

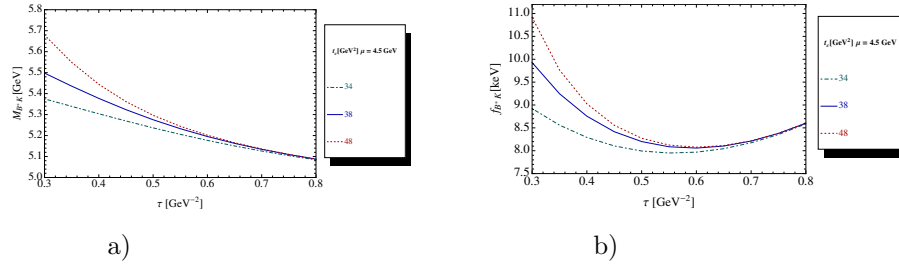


Fig. 4. **a)** M_{B^*K} at N2LO as function of τ for different values of t_c , $\mu = 4.5$ GeV and for the QCD parameters in Tables 2 and 3; **b)** The same as a) but for the coupling f_{B^*K} .

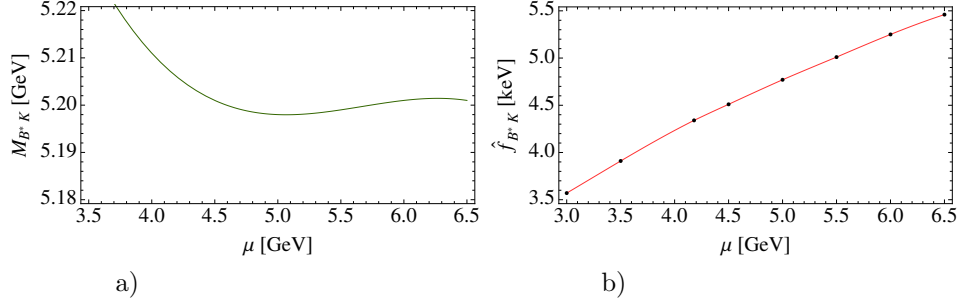


Fig. 5. **a)** M_{B^*K} at NLO as function of μ , for the corresponding τ -stability region, for $t_c \simeq 48 \text{ GeV}^2$ and for the QCD parameters in Tables 2 and 3; **b)** The same as a) but for the renormalization group invariant coupling \hat{f}_{B^*K} .

7.4. μ -subtraction point stability

We show in Fig. 5 the dependence of the results obtained at NLO of PT series on the choice of the subtraction constant μ . One can notice that the position of the τ -stability moves slightly with μ and is in the range of 0.50 to 0.66 GeV^{-2} . For each corresponding value of τ -stability, a minimum in μ is obtained around 5 GeV for the mass and a slight inflexion point at $\mu \simeq (4.5 \sim 5.0) \text{ GeV}$ for the renormalization group invariant coupling defined in Eq. 10, at which we extract the optimal estimate:

$$M_{B^*K}^{NLO} \simeq (5201 \sim 5198) \text{ MeV} \quad \text{and} \quad \hat{f}_{B^*K}^{NLO} \simeq (4.51 \sim 4.77) \text{ keV} . \quad (29)$$

7.5. Test of the convergence of the PT series

- We show, in Fig. 6a and 6b, the behaviour of the results for a given value of t_c for different truncation of the PT series. One can notice small PT corrections from LO to N2LO for the mass predictions as these corrections tend to compensate in the ratio of sum rules. There is also a good convergence of the PT series for the coupling prediction.

- The good convergence of the PT series indicate that the HO corrections dual to the tachyonic gluon one are negligible.

- It also validates (*a posteriori*) the results obtained at LO using the running b -quark mass as input as usually done in the existing literature.

7.6. Test of the convergence of the OPE

We test the convergence of the OPE by adding the contribution of the $d = 7$ condensate given in Eq. 13 and allowing a violation of factorization up to a factor $\chi = 4$. We see its effect in Fig. 7 where the coupling is largely affected while the one on the mass is almost negligible. Taking the maximal error corresponding to $\chi = 4$ and $t_c \simeq (34 \sim 48) \text{ GeV}^2$, we estimate the error due to the truncation of the OPE as:

$$\Delta f_{B^*K}^{OPE} \simeq \pm 1.98 \text{ keV} , \quad \Delta M_{B^*K}^{OPE} \simeq \pm 3 \text{ MeV} . \quad (30)$$

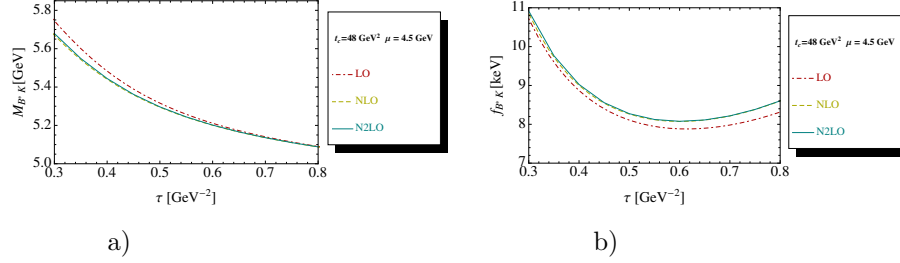
14 *R.M. Albuquerque et al.*


Fig. 6. **a)** M_{B^*K} as function of τ for different truncation of the PT series at a given value of $t_c=48$ GeV^2 , $\mu = 4.5$ GeV and for the QCD parameters in Tables 2 and 3; **b)** The same as a) but for the coupling f_{B^*K} .

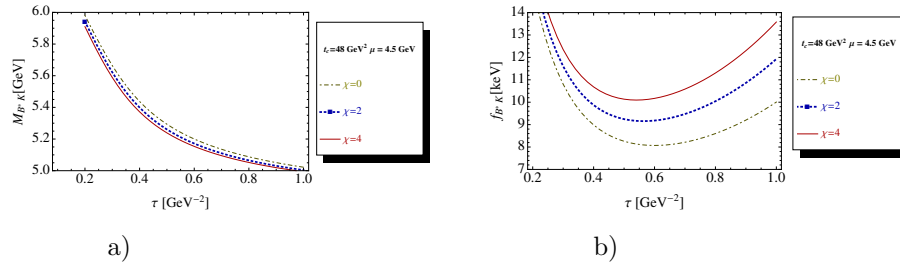


Fig. 7. **a)** M_{B^*K} as function of τ , for different values of the $d = 7$ condensate contribution (χ measures the violation of factorization), at a given value of $t_c=48$ GeV^2 , $\mu = 4.5$ GeV and for the QCD parameters in Tables 2 and 3; **b)** The same as a) but for the coupling f_{B^*K} .

7.7. Final results and error estimates

We show in Table 4 our estimate of the different sources of errors. The main errors from the mass come from the localisation of the τ and μ stabilities and to lesser extent from the QCD input parameters: α_s , $\langle \bar{q}q \rangle^2$ and the $SU(3)$ breaking parameter $\kappa \equiv \langle \bar{s}s \rangle / \langle \bar{q}q \rangle$. Adding quadratically different sources of errors, we consider as final estimate to order α_s^2 or at N2LO of the perturbative series and for $\mu = 4.5$ GeV :

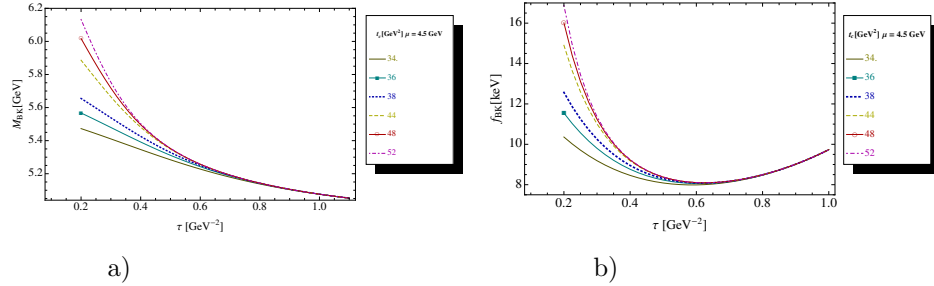
$$\begin{aligned} M_{B^*K} &\simeq (5186 \pm 13) \text{ MeV} , \\ \hat{f}_{B^*K} &\simeq (4.48 \pm 1.45) \text{ keV} \implies f_{B^*K}(4.5) \simeq (8.02 \pm 2.60) \text{ keV} . \end{aligned} \quad (31)$$

One can notice that the B^*K molecule mass (if any) is expected to be much below the physical B^*K threshold of 5818 MeV.

8. Mass and coupling of the BK (0^+) scalar molecule

Table 4. Different sources of errors for the estimate of the molecule masses (in units of MeV) and couplings (in units of keV) in the b -quark channel.

Inputs [GeV] ^d	ΔM_{B^*K}	Δf_{B^*K}	ΔM_{BK}	Δf_{BK}	$\Delta M_{B_s^*\pi}$	$\Delta f_{B_s^*\pi}$	$\Delta M_{B_s\pi}$	$\Delta f_{B_s\pi}$
<i>LSR parameters</i>								
$t_c = (34 \sim 48)$	1	0.01	1	0.06	2	0.09	0.001	0.08
$\mu = (4.5 \sim 5.0)$	2	0.40	1	0.60	3	0.30	3	0.8
$\tau = (\tau_{min} \pm 0.02)$	10	0.06	12	0.01	15	0.01	23	0.06
<i>QCD inputs</i>								
\bar{m}_b	0.83	0.023	0.83	0.023	0.85	0.03	0.83	0.03
\bar{m}_s	0.17	0.022	0.30	0.020	0.30	0.03	0.30	0.03
α_s	5.51	0.18	5.48	0.19	5.65	0.22	5.51	0.22
$\langle \bar{q}q \rangle$	0.38	0.006	0.32	0.007	0.20	0.002	0.18	0.002
κ	4.68	0.93	5.14	0.98	0.84	0.009	0.75	0.007
$\langle \alpha_s G^2 \rangle$	0.96	0.015	1.07	0.016	0.77	0.01	0.77	0.01
M_0^2	1.43	0.052	1.0	0.046	0.79	0.02	0.54	0.02
$\langle \bar{q}q \rangle^2$	2.97	1.28	2.76	1.32	2.78	1.50	1.81	1.53
$\langle g^2 G^3 \rangle$	0.0	0.0	0.0	0.0	0.0	0.0	0.0	0.0
$d \geq 7$	3.0	1.98	5.0	1.66	5	1.8	1.0	1.48
<i>Total errors</i>	13.4	2.6	15.4	2.4	17.7	2.40	24.0	2.3

Fig. 8. **a)** M_{BK} at LO as function of τ for different values of t_c , $\mu = 4.5$ GeV and for the QCD parameters in Tables 2 and 3; **b)** The same as a) but for the coupling f_{BK} .

8.1. τ - and t_c - stability criteria at lowest order (LO)

We redo the previous analysis for the BK scalar molecule. The results are shown in Fig. 8. For $\tau \simeq (0.55 - 0.60)$ GeV^{-2} where the coupling presents a τ -minimum, one obtains for $t_c \simeq (34 \sim 48)$ GeV^2 :

$$f_{BK}^{LO} \simeq (8.07 \sim 8.21) \text{ keV} . \quad (32)$$

For the mass, one obtains an inflexion point for $t_c \simeq (34 \sim 48)$ GeV^2 and for $\tau \simeq 0.60$ GeV^{-2} which corresponds to:

$$M_{BK}^{LO} \simeq (5250 \sim 5260) \text{ MeV} . \quad (33)$$

8.2. b -quark mass ambiguity at lowest order (LO)

We show in Fig. 9 the comparison of the result when we use the b -quark pole mass value of 4.66 GeV ⁶⁶ and the running mass $\bar{m}_b(m_b) = 4.18$ GeV in Table 2. One can

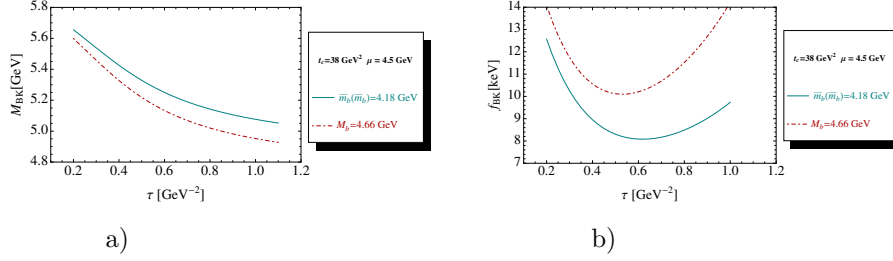
16 *R.M. Albuquerque et al.*

Fig. 9. **a)** M_{BK} at LO as function of τ for a given value of $t_c = 38 \text{ GeV}^2$, $\mu = 4.5 \text{ GeV}$ and for the QCD parameters in Tables 2 and 3; The OPE is truncated at $d = 6$. We compare the effect of the on-shell or pole mass $M_b = 4.66 \text{ GeV}$ and of the running mass $\bar{m}_b(\bar{m}_b) = 4.18 \text{ GeV}$; **b)** The same as a) but for the coupling f_{BK} .

find that this choice introduces an intrinsic source of error :

$$\Delta M_{BK}^{LO} \simeq 120 \text{ MeV} \quad \text{and} \quad \Delta f_{BK}^{LO} \simeq 2.1 \text{ keV} , \quad (34)$$

which should be added in the error when one does the LO analysis.

8.3. Higher order perturbative QCD corrections

- We improve the previous LO results by including $\mathcal{O}(\alpha_s)$ (NLO) and $\mathcal{O}(\alpha_s^2)$ (N2LO) corrections to the LO perturbative expression. The NLO analysis is shown in Fig. 10 versus τ , for $\mu = 4.5 \text{ GeV}$ and for different values of t_c . We obtain at the optimal stability point $\tau = (0.56 \sim 0.62) \text{ GeV}^{-2}$ and for $t_c \simeq (34 \sim 48) \text{ GeV}^2$:

$$M_{BK}^{NLO} \simeq (5205 \sim 5207) \text{ MeV} \quad \text{and} \quad f_{BK}^{NLO}(4.5) \simeq (8.14 \sim 8.27) \text{ keV} . \quad (35)$$

- Adding the N2LO corrections, one obtains similar behaviours as in Fig 10. In this case, the results become:

$$M_{BK}^{N2LO} \simeq 5195 \text{ GeV} \quad \text{and} \quad f_{BK}^{N2LO}(4.5) \simeq (8.18 \sim 8.30) \text{ keV} , \quad (36)$$

where one can notice tiny corrections from NLO to N2LO implying also a negligible correction tachyonic gluon mass contribution.

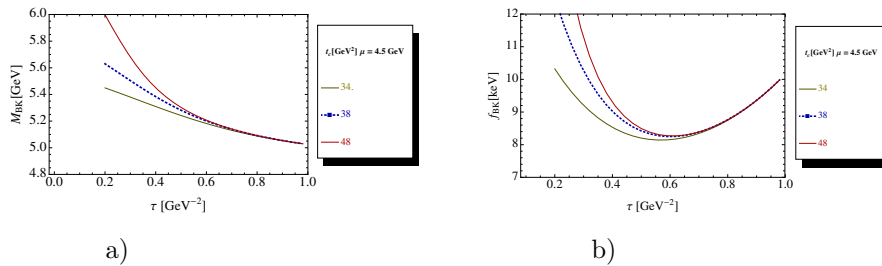


Fig. 10. **a)** M_{BK} at NLO as function of τ for different values of t_c , for $\mu = 4.5 \text{ GeV}$ and for the QCD parameters in Tables 2 and 3; **b)** The same as a) but for the coupling f_{BK} .

8.4. μ - subtraction point stability

We show in Fig. 11 the dependence of M_{BK} and of the renormalization group invariant coupling \hat{f}_{BK} obtained at NLO of PT series on the choice of the subtraction constant μ . We consider as optimal values the ones obtained for $\mu \simeq (4.5 - 5.0)$ GeV where we have almost a plateau for the mass and a slight inflexion point for \hat{f}_{BK} . We deduce:

$$M_{BK}^{NLO}(\mu) \simeq (5207 \sim 5205) \text{ MeV} \quad \text{and} \quad \hat{f}_{BK}^{NLO}(\mu) \simeq (2.58 \sim 2.68) \text{ keV} . \quad (37)$$

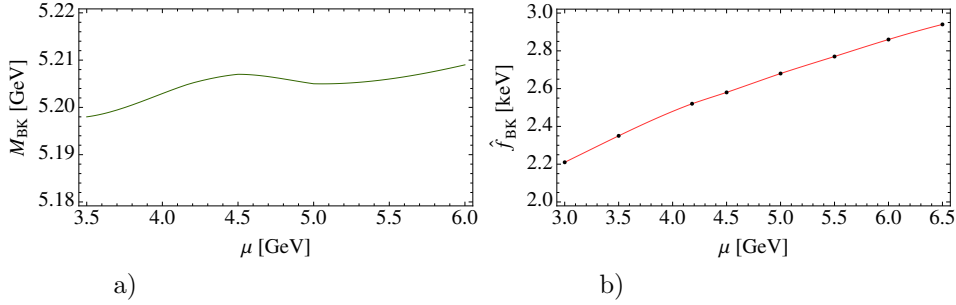


Fig. 11. **a)** M_{BK} at NLO as function of μ , for the corresponding τ -stability region, for $t_c \simeq 48 \text{ GeV}^2$ and for the QCD parameters in Tables 2 and 3; **b)** The same as a) but for the renormalization group invariant coupling \hat{f}_{BK} .

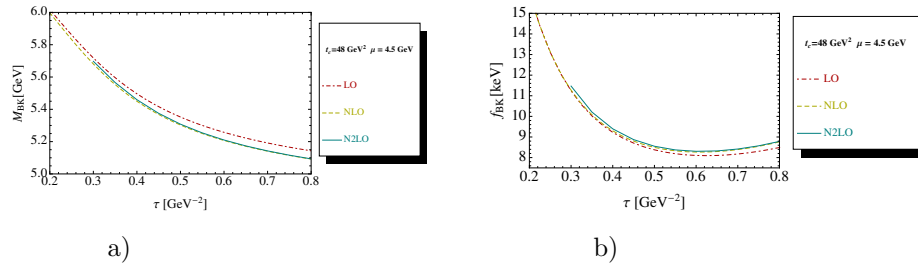


Fig. 12. **a)** M_{BK} as function of τ for different truncation of the PT series at a given value of $t_c=48 \text{ GeV}^2$, $\mu = 4.5 \text{ GeV}$ and for the QCD parameters in Tables 2 and 3; **b)** The same as a) but for the coupling f_{BK} .

8.5. Test of the convergence of the PT series

We show in Fig. 12 the behaviour of the results for a given value of t_c and of μ and for different truncation of the PT series. One can notice small PT corrections for the mass predictions because these corrections tend to compensate in the ratio of sum rules. For the coupling, the correction is large from LO to NLO. For both observables, one can notice a good convergence of the PT series from NLO to N2LO.

8.6. Test of the convergence of the OPE

We show the effect of a class of the $d = 7$ condensate for different values of χ in Fig. 13. Taking the maximal error corresponding to $\chi = 4$, we estimate the error due to the truncation of the OPE as:

$$\Delta f_{BK}^{OPE} \simeq \pm 1.66 \text{ keV} , \quad \Delta M_{BK}^{OPE} \simeq \pm 5 \text{ MeV} . \quad (38)$$

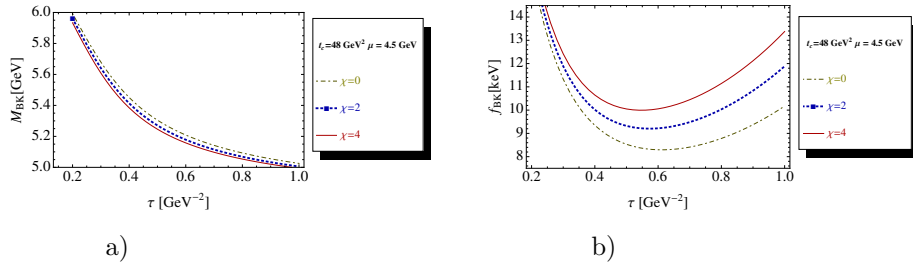


Fig. 13. **a)** M_{BK} as function of τ , for different values of the $d = 7$ condensate contribution (χ measures the violation of factorization), at a given value of $t_c=48 \text{ GeV}^2$, $\mu = 4.5 \text{ GeV}$ and for the QCD parameters in Tables 2 and 3; **b)** The same as a) but for the coupling f_{BK} .

8.7. Final results and comparison with previous estimates

- We show in Table 4 our estimate of the different sources of errors. Like in the case of B^*K , the main errors from the mass come from the localisation of the τ -stability, α_s , $\kappa \equiv \langle \bar{s}s \rangle / \langle \bar{q}q \rangle$, $\langle \bar{q}q \rangle^2$ and M_0^2 . Adding quadratically different sources of errors, we consider as a final estimate to order α_s^2 or at N2LO of the perturbative series and including an estimate of the $d \geq 7$ dimension condensates:

$$\begin{aligned} \hat{f}_{BK} &\simeq (2.57 \pm 0.75) \text{ keV} \implies f_{BK}(4.5) \simeq (8.26 \pm 2.40) \text{ keV} , \\ M_{BK} &\simeq (5195 \pm 15) \text{ MeV} . \end{aligned} \quad (39)$$

for $\mu = 4.5 \text{ GeV}$.

- One can notice that the BK molecule mass (if any) is about 11 MeV heavier than the B^*K molecule and below the physical BK threshold of 5773 MeV.

- Comparing numerically the QCD expression of our spectral function with the one in,¹⁴ one finds that the perturbative (PT) and $\langle \bar{q}q \rangle$ expressions have wrong signs^g a good agreement except for the $\langle \bar{q}q \rangle^2$ condensate contributions which coefficient is too small compared to ours.

- As mentioned previously, we refrain to add the condensate contributions of dimension higher than $d = 6$ due to the large uncertainties on the values of these

^gThe negative sign of the PT contribution violates the general positive property of the spectral function. The same wrong sign occurs in Ref. ¹⁵

high-dimension condensates (violation of factorization) and to the fact that the contributions of these condensates correspond only to one class of diagrams of the OPE but not to the complete contributions. However, we have seen previously that the effect of the $d = 7$ condensates is negligible in the present channel.

• Our result differs from the LO one in¹⁴ who found the mass $M_{BK} = 5584(137)$ MeV. One can understand the source of the discrepancy as the result of Ref.¹⁴ has been obtained for the sum rule variable $M^2 = (3 \sim 6) \text{ GeV}^2$ or equivalently for $\tau \equiv 1/M^2 \simeq (0.17 \sim 0.33) \text{ GeV}^{-2}$ which is outside the τ -stability region of about 0.6 GeV^{-2} (inflexion point for the mass and minimum for the coupling) as clearly shown in Fig. 8. In addition to the sensitivity on the variation of τ^h , one can notice that, in this small τ -region, the result is also very sensitive to the choice of the continuum threshold t_c such that the prediction becomes unreliable.

9. B^*K/BK ratio from Double Ratio of Sum Rule (DRSR)

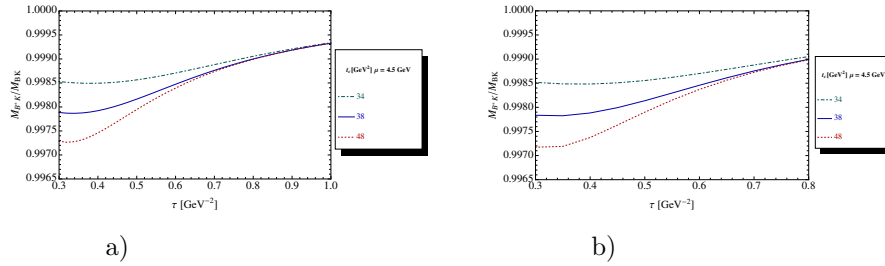


Fig. 14. **a)** M_{B^*K}/M_{BK} at LO as function of τ for different values of t_c , for $\mu = 4.5 \text{ GeV}$ and for the QCD parameters in Tables 2 and 3; **b)** The same as a) but at N2LO.

We cross-check the previous result by a direct estimate of the B^*K/BK mass and

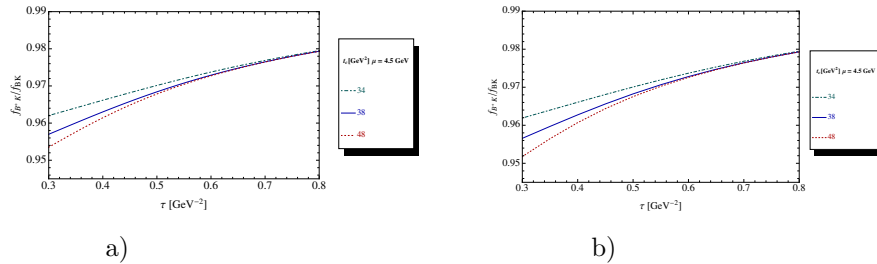


Fig. 15. **a)** f_{B^*K}/f_{BK} at LO as function of τ for different values of t_c , for $\mu = 4.5 \text{ GeV}$ and for the QCD parameters in Tables 2 and 3; **b)** The same as a) but at N2LO.

coupling ratios using the Double Ratio of Sum Rule (DRSR).²² As explicitly seen

^hThe apparent stability shown in¹⁴ comes from the scale chosen for the figure frame.

20 *R.M. Albuquerque et al.*

in,^{24–33} DRSR has the advantage to be free from systematic uncertainties, to be less sensitive to the PT and non-perturbative (NPT) corrections if they act in the same signs in the two channels. The results of the analysis are shown in Figs. 14 and 15. One can see that there is not a good stability in τ though the results change slightly with it. Taking $\tau \simeq 0.6 \text{ GeV}^{-2}$ where the ratio of sum rules predicting the absolute value of the coupling and masses stabilizes, one deduces at N2LO for $t_c \simeq (34 \sim 48) \text{ GeV}^2$:

$$M_{B^*K}/M_{BK} \simeq (0.999 \sim 0.998) , \quad \text{and} \quad f_{B^*K}/f_{BK} \simeq (0.973 \sim 0.972) . \quad (40)$$

Using the value of M_{BK} and f_{BK} in Eq. 39, one can deduce:

$$M_{B^*K} \simeq (5187 \pm 15) \text{ MeV} , \quad \text{and} \quad f_{B^*K} \simeq (8.03 \pm 1.71) \text{ keV} , \quad (41)$$

which confirms the previous estimates in Eq. 31.

10. Spectral functions of the $B_s^*\pi$ and $B_s\pi$ molecules

10.1. $B_s^*\pi$ (1^+) *axial-vector molecule*

We shall also consider the two-point spectral function associated to the molecule $B_s\pi$ state with the current given in Table 1. Its QCD expression reads to lowest order:

$$\begin{aligned} \rho^{pert} &= \frac{M_b^8}{5 \cdot 2^{14} \pi^6} \left[\frac{5}{x^4} - \frac{96}{x^3} - \frac{945}{x^2} + \frac{480}{x} - 60 \left(\frac{9}{x^2} + \frac{16}{x} + 3 \right) \text{Log } x + 555 + x^2 \right] + \\ &\quad \frac{m_s M_b^7}{2^{12} \pi^6} \left[\frac{1}{x^3} + \frac{28}{x^2} + 12 \left(\frac{1}{x^2} + \frac{3}{x} + 1 \right) \text{Log } x - 28 - x \right] , \\ \rho^{\langle \bar{q}q \rangle} &= -\frac{M_b^5}{2^8 \pi^4} \kappa \langle \bar{q}q \rangle \left[\frac{1}{x^2} + \frac{9}{x} + 6 \left(\frac{1}{x} + 1 \right) \text{Log } x - 9 - x \right] + \\ &\quad \frac{m_s M_b^4}{2^{11} \pi^4} \kappa \langle \bar{q}q \rangle \left(\frac{3}{x^2} - \frac{16}{x} - 12 \text{Log } x + 12 + x^2 \right) ; \\ \rho^{\langle G^2 \rangle} &= \frac{M_b^4}{3 \cdot 2^{15} \pi^6} 4\pi \langle \alpha_s G^2 \rangle \left[\frac{1}{x^2} - \frac{120}{x} - 12 \left(\frac{4}{x} + 7 \right) \text{Log } x + 108 + 8x + 3x^2 \right] , \\ \rho^{\langle \bar{q}Gq \rangle} &= \frac{3M_b^3}{2^9 \pi^4} \kappa \langle \bar{q}Gq \rangle \left(\frac{1}{x} + 2 \text{Log } x - x \right) - \frac{m_s M_b^2}{2^{10} \pi^4} \kappa \langle \bar{q}Gq \rangle \left(\frac{4}{x} + 6 \text{Log } x - 1 - 4x + x^2 \right) , \\ \rho^{\langle \bar{q}q \rangle^2} &= \frac{M_b^2}{3 \cdot 2^5 \pi^2} \rho \langle \bar{q}q \rangle^2 \left(\frac{2}{x} - 3 + x^2 \right) + \frac{m_s M_b}{2^4 \pi^2} \rho \langle \bar{q}q \rangle^2 (1 - x) \\ \rho^{\langle G^3 \rangle} &= \frac{M_b^2}{3^2 \cdot 2^{17} \pi^6} \langle g^3 G^3 \rangle \left[\frac{9}{x^2} - \frac{160}{x} - 12 \left(\frac{4}{x} + 9 \right) \text{Log } x + 144 + 7x^2 \right] \end{aligned} \quad (42)$$

The contribution of a class of $d = 7$ condensate for $m_s = 0$ is:

$$\rho^{\langle \bar{q}q \rangle \langle G^2 \rangle} = -\frac{M_b \kappa \langle \bar{q}q \rangle}{3 \cdot 2^9 \pi^4} 4\pi \langle \alpha_s G^2 \rangle \left(\frac{1}{x} + 3 \text{Log } x + 5 - 6x \right) . \quad (43)$$

10.2. $B_s\pi$ scalar molecule

The expression of the $B_s\pi$ scalar two-point spectral function associated to the molecule state with the current given in Table 1 reads to lowest order:

$$\begin{aligned}
\rho^{pert} &= \frac{M_b^8}{5 \cdot 2^{14} \pi^6} \left[\frac{1}{x^4} - \frac{20}{x^3} - \frac{220}{x^2} + \frac{80}{x} - 60 \left(\frac{2}{x^2} + \frac{4}{x} + 1 \right) \text{Log } x + 155 + 4x \right] + \\
&\quad \frac{m_s M_b^7}{2^{12} \pi^6} \left[\frac{1}{x^3} + \frac{28}{x^2} + 12 \left(\frac{1}{x^2} + \frac{3}{x} + 1 \right) \text{Log } x - 28 - x \right], \\
\rho^{\langle \bar{q}q \rangle} &= -\frac{M_b^5}{2^8 \pi^4} \kappa \langle \bar{q}q \rangle \left[\frac{1}{x^2} + \frac{9}{x} + 6 \left(\frac{1}{x} + 1 \right) \text{Log } x - 9 - x \right] + \\
&\quad \frac{m_s M_b^4}{2^9 \pi^4} \kappa \langle \bar{q}q \rangle \left(\frac{1}{x^2} - \frac{6}{x} - 6 \text{Log } x + 3 + 2x \right); \\
\rho^{\langle G^2 \rangle} &= \frac{M_b^4}{3 \cdot 2^{13} \pi^6} 4\pi \langle \alpha_s G^2 \rangle \left[\frac{5}{x^2} + 6 \left(\frac{2}{x} - 1 \right) \text{Log } x - 9 + 4x \right], \\
\rho^{\langle \bar{q}Gq \rangle} &= \frac{3M_b^3}{2^8 \pi^4} \kappa \langle \bar{q}Gq \rangle \left[\frac{3}{x} + \left(\frac{1}{x} + 3 \right) \text{Log } x - 2 - x \right] + \\
&\quad \frac{m_s M_b^2}{2^8 \pi^4} \kappa \langle \bar{q}Gq \rangle \left(\frac{1}{x} + 3 \text{Log } x + 1 - 2x \right), \\
\rho^{\langle \bar{q}q \rangle^2} &= \frac{M_b^2}{2^5 \pi^2} \rho \langle \bar{q}q \rangle^2 \left(\frac{1}{x} - 2 + x \right) + \frac{m_s M_b}{2^4 \pi^2} \rho \langle \bar{q}q \rangle^2 (1 - x) \\
\rho^{\langle G^3 \rangle} &= \frac{M_b^2}{3 \cdot 2^{15} \pi^6} \langle g^3 G^3 \rangle \left[\frac{1}{x^2} - \frac{21}{x} - 6 \left(\frac{1}{x} + 3 \right) \text{Log } x + 15 + 5x \right] \quad (44)
\end{aligned}$$

The contribution of a class of $d = 7$ condensate for $m_s = 0$ is:

$$\rho^{\langle \bar{q}q \rangle \langle G^2 \rangle} = -\frac{M_b \kappa \langle \bar{q}q \rangle}{3 \cdot 2^9 \pi^4} 4\pi \langle \alpha_s G^2 \rangle \left(\frac{1}{x} + 12 \text{Log } x + 14 - 15x \right). \quad (45)$$

11. Mass and coupling of the $B_s^*\pi$ (1^+) axial-vector molecule

11.1. τ - and t_c -stability criteria at lowest order (LO)

The results of the analysis are shown in Fig. 16. For $\tau \simeq (0.58 - 0.62)$ GeV $^{-2}$ where the coupling presents a τ -minimum and the mass an inflexion point, one obtains for $t_c \simeq (34 \sim 48)$ GeV 2 :

$$f_{B_s^*\pi}^{LO} \simeq (9.41 \sim 9.55) \text{ keV} \quad \text{and} \quad M_{B_s^*\pi}^{LO} \simeq 5208 \text{ MeV}. \quad (46)$$

11.2. b -quark mass ambiguity at lowest order (LO)

In Fig. 17, we show the influence on the choice of the quark mass value on the coupling and mass at lowest order. One can see an effect of about 2.2 keV (23%)

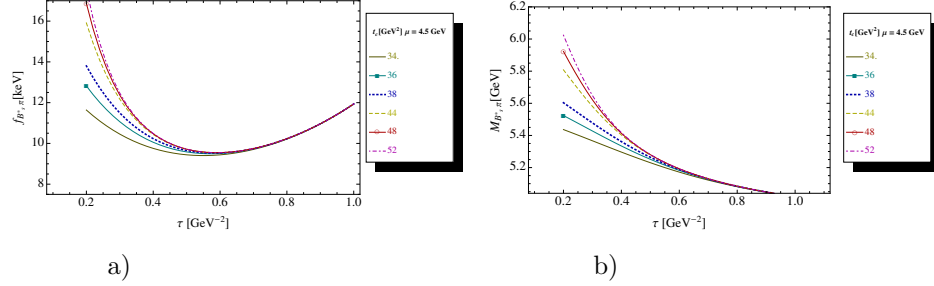
22 *R.M. Albuquerque et al.*


Fig. 16. **a)** $f_{B_s^*\pi}$ at LO as function of τ for different values of t_c , $\mu = 4.5$ GeV and for the QCD parameters in Tables 2 and 3; **b)** The same as a) but for the mass.

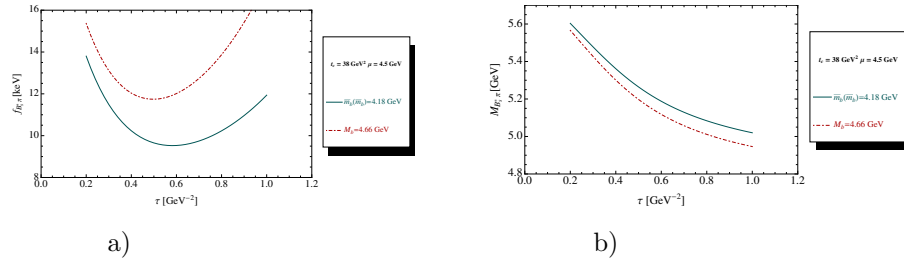


Fig. 17. **a)** $f_{B_s^*\pi}$ at LO as function of τ for a given value of $t_c = 38$ GeV^2 , $\mu = 4.5$ GeV and for the QCD parameters in Tables 2 and 3; The OPE is truncated at $d = 6$. We compare the effect of the on-shell or pole mass $\bar{m}_b = 4.66$ GeV and of the running mass $\bar{m}_b(\bar{m}_b) = 4.18$ GeV; **b)** The same as a) but for the mass.

for the coupling and about 4 MeV for the mass $M_{B_s^*\pi}$.

11.3. μ -dependence of the result at NLO

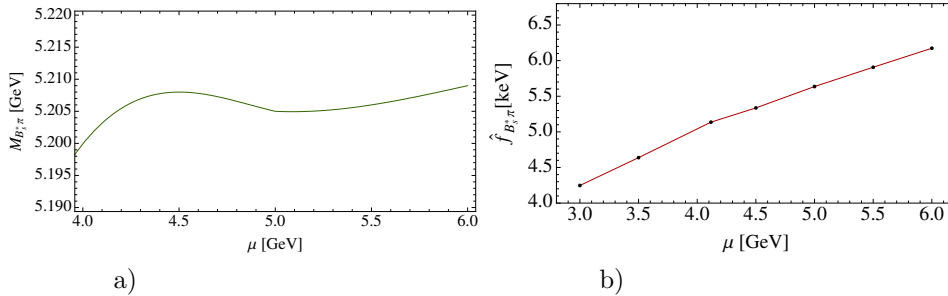


Fig. 18. **a)** $M_{B_s^*\pi}$ at NLO as function of μ , for the corresponding τ -stability region, for $t_c \simeq 48$ GeV^2 and for the QCD parameters in Tables 2 and 3; **b)** The same as a) but for the renormalization group invariant coupling $\hat{f}_{B_s^*\pi}$.

We study the μ -dependence of the result including α_s -corrections.

11.4. Test of the convergence of the PT series

We show in Fig. 19 the behaviour of the results for a given value of t_c and of μ and for different truncation of the PT series. One can notice small PT corrections for the mass and coupling predictions.

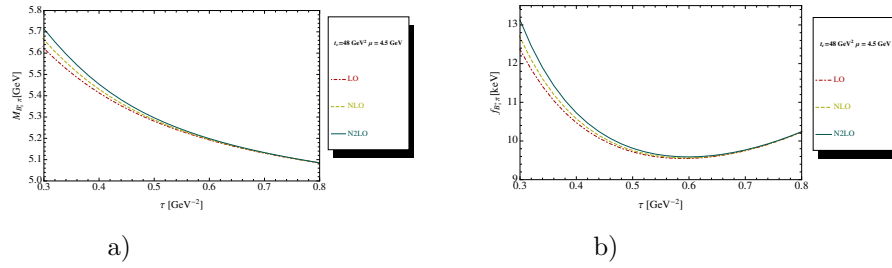


Fig. 19. **a)** $M_{B_s^* \pi}$ as function of τ for different truncation of the PT series at a given value of $t_c=48$ GeV^2 , $\mu = 4.5$ GeV and for the QCD parameters in Tables 2 and 3; **b)** The same as a) but for the coupling $f_{B_s^* \pi}$.

11.5. Error induced by the OPE

Like in previous section, we estimate this effect by taking a violation of about a factor 4 of the factorization assumption for the $d = 7$ condensates. The analysis is shown in Fig. 20 from which we deduce:

$$\Delta f_{B_s^* \pi}^{OPE} \simeq \pm 1.80 \text{ keV} , \quad \Delta M_{B_s^* \pi}^{OPE} \simeq \pm 5 \text{ MeV} . \quad (47)$$

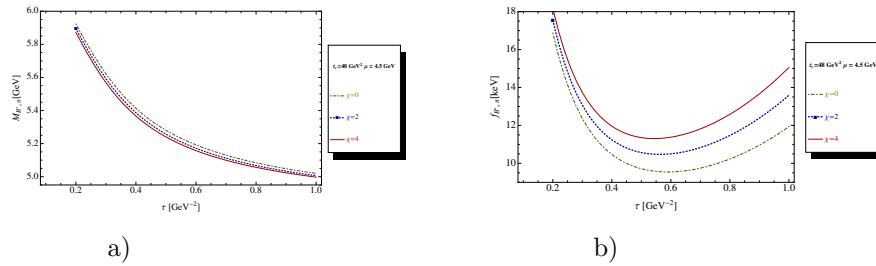


Fig. 20. **a)** $M_{B_s^* \pi}$ as function of τ , for different values of the $d = 7$ condensate contribution (χ measures the violation of factorization), at a given value of $t_c=48$ GeV^2 , $\mu = 4.5$ GeV and for the QCD parameters in Tables 2 and 3; **b)** The same as a) but for the coupling $f_{B_s^* \pi}$.

11.6. Final results at N2LO

We conclude from the previous analysis the results at N2LO and for $\mu = 5$ GeV:

$$\begin{aligned} M_{B_s^* \pi} &\simeq (5200 \pm 18) \text{ MeV} , \\ \hat{f}_{B_s^* \pi} &\simeq (5.61 \pm 1.32) \text{ keV} \implies f_{B_s^* \pi}(4.5) \simeq (10.23 \pm 2.40) \text{ keV} . \end{aligned} \quad (48)$$

12. Mass and coupling of the $B_s \pi$ (0^+) scalar molecule

12.1. τ - and t_c -stability criteria at lowest order (LO)

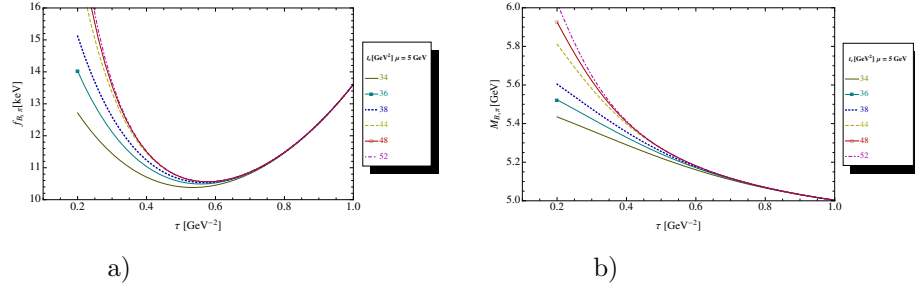


Fig. 21. **a)** $f_{B_s \pi}$ at LO as function of τ for different values of t_c , $\mu = 4.5$ GeV and for the QCD parameters in Tables 2 and 3; **b)** The same as a) but for the mass $M_{B_s \pi}$.

The results of the analysis are shown in Fig. 21. For $\tau \simeq (0.58 - 0.62) \text{ GeV}^{-2}$ where the coupling presents a τ -minimum and the mass an inflexion point, one obtains for $t_c \simeq (34 \sim 48) \text{ GeV}^2$:

$$f_{B_s \pi}^{LO} \simeq (9.65 \sim 9.80) \text{ keV} \quad \text{and} \quad M_{B_s \pi}^{LO} \simeq (5234 \sim 5235) \text{ MeV} . \quad (49)$$

12.2. b -quark mass ambiguity at lowest order (LO)

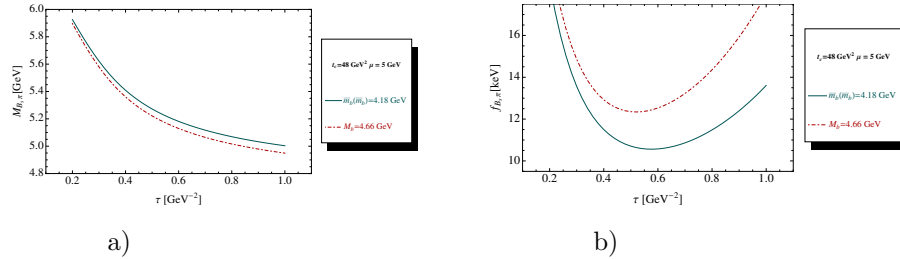


Fig. 22. **a)** $f_{B_s \pi}$ at LO as function of τ for a given value of $t_c = 48 \text{ GeV}^2$, $\mu = 4.5$ GeV and for the QCD parameters in Tables 2 and 3; The OPE is truncated at $d = 6$. We compare the effect of the on-shell or pole mass $M_b = 4.66 \text{ GeV}$ and of the running mass $\bar{m}_b(\bar{m}_b) = 4.18 \text{ GeV}$; **b)** The same as a) but for the mass $M_{B_s \pi}$.

In Fig. 22, we show the influence on the choice of the quark mass value on the coupling and mass at lowest order. One can see an effect of about 27% for the coupling and about 5% for the mass.

12.3. μ -subtraction point stability

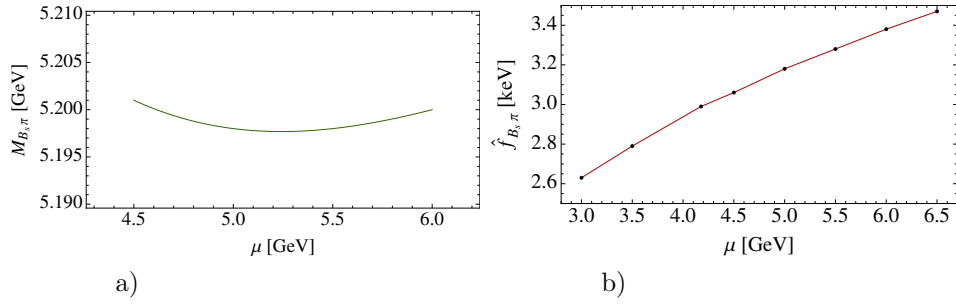


Fig. 23. **a)** $M_{B_s\pi}$ at NLO as function of μ , for the corresponding τ -stability region, for $t_c \simeq 48 \text{ GeV}^2$ and for the QCD parameters in Tables 2 and 3; **b)** The same as a) but for the renormalization group invariant coupling $\hat{f}_{B_s\pi}$.

We show in Fig. 23 the dependence of $M_{B_s\pi}$ and of the renormalization group invariant coupling $\hat{f}_{B_s\pi}$ obtained at NLO of PT series on the choice of the subtraction constant μ . We consider as an optimal values the ones obtained for $\mu \simeq 5.0 \text{ GeV}$ where we have a minimum for the mass and a slight inflexion point for $\hat{f}_{B_s\pi}$. We deduce for $t_c \simeq (34 \sim 48) \text{ GeV}^2$:

$$M_{B_s\pi}^{NLO}(\mu) \simeq (5196 \sim 5198) \text{ MeV} \quad \text{and} \quad \hat{f}_{B_s\pi}^{NLO}(\mu) \simeq (3.12 \sim 3.18) \text{ keV} . \quad (50)$$

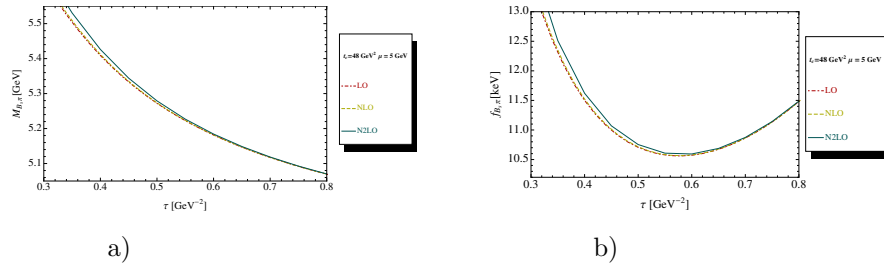


Fig. 24. **a)** $M_{B_s\pi}$ as function of τ for different truncation of the PT series at a given value of $t_c=48 \text{ GeV}^2$, $\mu = 4.5 \text{ GeV}$ and for the QCD parameters in Tables 2 and 3; **b)** The same as a) but for the coupling $f_{B_s\pi}$.

12.4. Test of the convergence of the PT series

We show in Fig. 24 the behaviour of the results for a given value of t_c and for different truncation of the PT series. One can notice small PT corrections for the mass predictions because these corrections tend to compensate in the ratio of sum rules. For the coupling, the correction is large from LO to NLO. For both observables, one can notice a good convergence of the PT series from LO to N2LO.

12.5. Error induced by the OPE

Like in previous section, we estimate this effect by taking a violation of about a factor 4 of the factorization assumption for the $d = 7$ condensates. The analysis is shown in Fig. 25 from which we deduce for $t_c \simeq (34 \sim 48) \text{ GeV}^2$:

$$\Delta f_{B_s\pi}^{OPE} \simeq \pm 1.48 \text{ keV} , \quad \Delta M_{B_s\pi}^{OPE} \simeq \pm 1 \text{ MeV} . \quad (51)$$

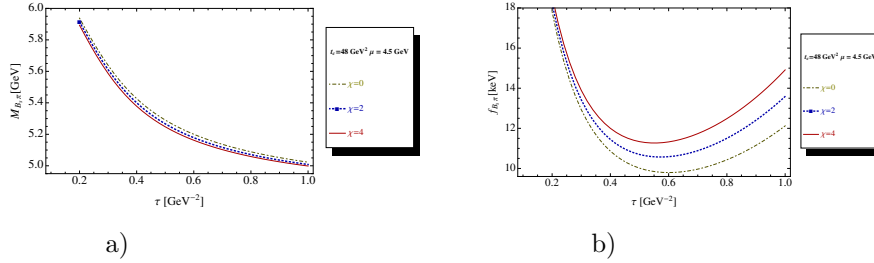


Fig. 25. **a)** $M_{B_s\pi}$ as function of τ , for different values of the $d = 7$ condensate contribution (χ measures the violation of factorization), at a given value of $t_c = 48 \text{ GeV}^2$, $\mu = 4.5 \text{ GeV}$ and for the QCD parameters in Tables 2 and 3; **b)** The same as a) but for the coupling $f_{B_s\pi}$.

12.6. Final results

We show in Table 4 our estimate of the different sources of errors. Adding quadratically the different sources of errors, we consider as a final estimate for $\mu = 5 \text{ GeV}$ and to order α_s^2 or at N2LO of the perturbative series:

$$M_{B_s\pi} \simeq (5199 \pm 24) \text{ MeV} , \quad \hat{f}_{B_s\pi} \simeq (3.15 \pm 0.70) \text{ keV} \quad \Rightarrow \quad f_{B_s\pi} \simeq (10.5 \pm 2.3) \text{ keV} , \quad (52)$$

which we list in Table 7. One can notice that the $B_s\pi$ molecule mass (if any) is also expected to be below the physical $B_s\pi$ threshold of 5500 MeV.

13. QCD expression of the 0^+ scalar four-quark $(su)(\bar{b}\bar{d})$ states

Using the expression of the vector current in Table 1, we deduce the expression of the scalar spectral function from the longitudinal part of the correlator.

$$\begin{aligned}
 \rho^{pert} &= \frac{(1+k^2)M_b^8}{5 \cdot 3 \cdot 2^{13} \pi^4} \left[\frac{1}{x^4} - \frac{16}{x^3} - \frac{65}{x^2} + \frac{160}{x} - 60 \left(\frac{1}{x^2} - 1 \right) \text{Log}(x) - 65 - 16x + x^2 \right], \\
 \rho^{\langle \bar{q}q \rangle} &= -\frac{(1-k^2)M_b^5}{3 \cdot 2^6 \pi^4} \langle \bar{q}q \rangle \left[\frac{1}{x^2} + \frac{9}{x} + 6 \left(\frac{1}{x} + 1 \right) \text{Log}(x) - 9 - x \right] \\
 &\quad - \frac{m_s m_b^4}{3 \cdot 2^9 \pi^4} \langle \bar{q}q \rangle \left[2(1-k^2) - (1+k^2)\kappa \right] \left[\frac{1}{x^2} + 12 \text{Log}(x) + 12 - 16x + 3x^2 \right], \\
 \rho^{\langle G^2 \rangle} &= \frac{(1+k^2)M_b^4}{3^2 \cdot 2^{13} \pi^6} 4\pi \langle \alpha_s G^2 \rangle \left[\frac{5}{x^2} + \frac{40}{x} + 24 \left(\frac{1}{x} + 2 \right) \text{Log}(x) - 18 - 32x + 5x^2 \right], \\
 \rho^{\langle \bar{q}Gq \rangle} &= \frac{(1-k^2)m_b^3}{2^7 \pi^4} \langle \bar{q}Gq \rangle \left[\frac{1}{x} + 2 \text{Log}(x) - x \right] \\
 &\quad + \frac{m_s M_b^2}{3 \cdot 2^8 \pi^4} \langle \bar{q}Gq \rangle (6(1-k^2) + (1+k^2)\kappa) (1-x)^2, \\
 \rho^{\langle \bar{q}q \rangle^2} &= \frac{(1-k^2)M_b^2}{3 \cdot 2^3 \pi^2} \rho^{\langle \bar{q}q \rangle} \kappa (1-x)^2 + \frac{m_s M_b}{3 \cdot 2^3 \pi^2} \rho^{\langle \bar{q}q \rangle^2} \left[2(1+k^2) - (1-k^2)\kappa \right] (1-x), \\
 \rho^{\langle G^3 \rangle} &= \frac{(1+k^2)M_b^2}{3^2 \cdot 2^{15} \pi^6} \langle g_s^3 G^3 \rangle \left[\frac{1}{x^2} + \frac{8}{x} + 36 \text{Log}(x) + 24 - 40x + 7x^2 \right]. \quad (53)
 \end{aligned}$$

The contribution of a class of $d = 7$ condensate for $m_s = 0$ is:

$$\rho^{\langle \bar{q}q \rangle \langle G^2 \rangle} = -(1-k^2) \frac{M_b \langle \bar{q}q \rangle}{3^2 \cdot 2^8 \pi^4} 4\pi \langle \alpha_s G^2 \rangle \left(\frac{2}{x} + 6 \text{Log} x + 7 - 9x \right). \quad (54)$$

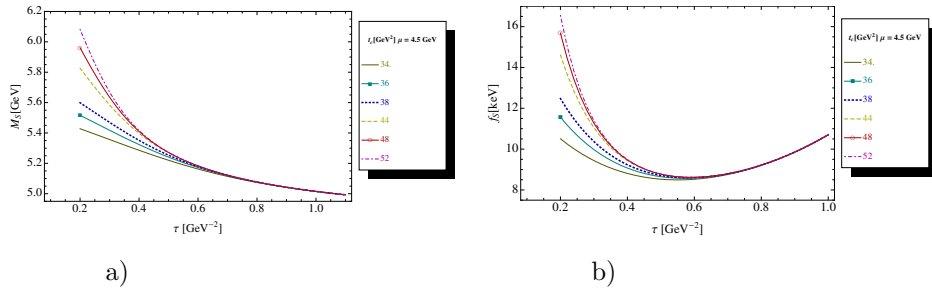


Fig. 26. **a)** M_{S_b} at LO as function of τ for different values of t_c , $\mu = 4.5$ GeV, mixing of currents $k = 0$ and for the QCD parameters in Tables 2 and 3; **b)** The same as a) but for the coupling f_S .

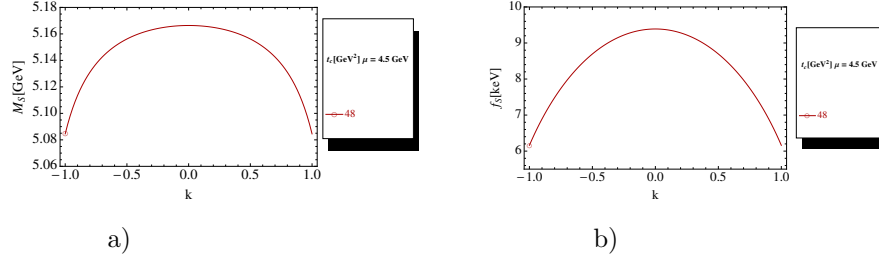
28 *R.M. Albuquerque et al.*


Fig. 27. **a)** M_{S_b} at LO as function of the mixing of currents k , for $\tau = 0.6 \text{ GeV}^{-2}$, $\mu = 4.5 \text{ GeV}$, $t_c = 48 \text{ GeV}^2$ and for the QCD parameters in Tables 2 and 3; **b)** The same as a) but for the coupling f_{S_b} .

14. Mass and coupling of the 0^+ scalar S_b four-quark state

14.1. τ - and t_c -stabilities

We study the τ - and t_c -stabilities of the mass and coupling predictions in Fig. 26 by fixing the subtraction point $\mu = 4.5 \text{ GeV}$ and the mixing of current k defined in Table 1 to be equal to zero. We have an inflexion point for the mass and a minimum for the coupling for $\tau \simeq (0.56 \sim 0.6) \text{ GeV}^{-2}$. This τ -stability is reached from $t_c \simeq 34 \text{ GeV}^2$ while t_c -stability is obtained around $t_c = 48 \text{ GeV}^2$.

14.2. Optimal choice of the four-quark currents

We show in Fig. 27 the behaviour of the mass and coupling predictions versus the mixing of current k defined in Table 1 given the value $\tau \simeq 0.6 \text{ GeV}^{-2}$, $\mu = 4.5 \text{ GeV}$, $t_c = 48 \text{ GeV}^2$ and for the QCD parameters in Table 2. One can notice that the optimal choice is obtained for $k = 0$ which can simply be understood analytically by taking the zero of the derivative of the spectral function versus k :

$$\frac{\partial \rho}{\partial k} = 0 \implies k = 0. \quad (55)$$

14.3. Lowest Order (LO) results

Therefore, to the LO approximation, we deduce from Fig. 26 at the stability region:

$$M_{S_b}^{LO} \simeq (5.19 \sim 5.18) \text{ GeV} \quad \text{and} \quad f_{S_b}^{LO} \simeq (8.49 \sim 8.62) \text{ keV}. \quad (56)$$

14.4. b -quark mass ambiguity at lowest order (LO)

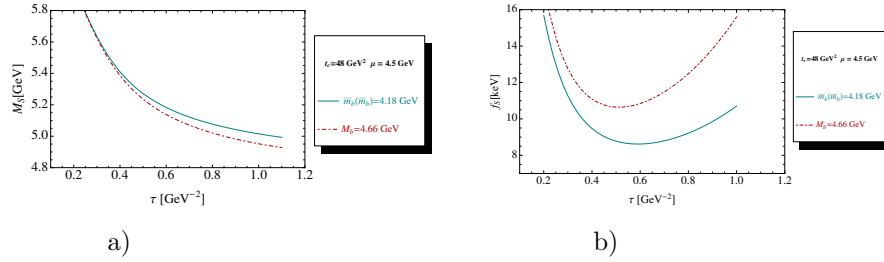
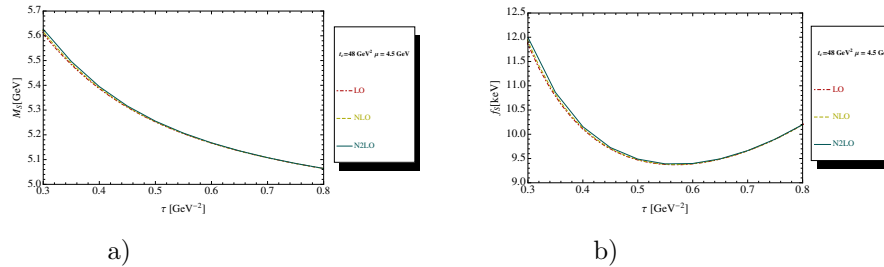
We compare in Fig. 28 the result when we use the b -quark pole mass value of 4.66 GeV ⁶⁶ and the running mass $\bar{m}_b(m_b) = 4.18 \text{ GeV}$ in Table 2. One can find that this (a priori) choice introduces an intrinsic source of error :

$$\Delta M_{S_b}^{LO} \simeq 43 \text{ MeV} \quad \text{and} \quad \Delta f_{S_b}^{LO} \simeq 2.6 \text{ keV}, \quad (57)$$

which should be added into the error when one does the LO analysis.

Table 5. Different sources of errors for the estimate of the axial-vector ($A_{b,c}$) and scalar four-quark ($S_{b,c}$) masses (in units of MeV) and couplings (in units of keV).

Inputs [GeV] ^d	ΔM_{S_b}	Δf_{S_b}	ΔM_{A_b}	Δf_{A_b}	ΔM_{S_c}	Δf_{S_c}	ΔM_{A_c}	Δf_{A_c}
<i>LSR parameters</i>								
$t_c^c = (12 \sim 18)$	—	—	—	—	0.5	2.7	7	2
$t_c^b = (34 \sim 48)$	4	0.16	2	0.12	—	—	—	—
$\mu^c = (2.0 \sim 2.5)$	—	—	—	—	0.5	11	9.5	15
$\mu^b = (4.5 \sim 5.0)$	1	0.34	6	0.36	—	—	—	—
$\tau = \tau_{min} \pm 0.02$	15	0.01	12	0.01	30	0.12	28	0.2
<i>QCD inputs</i>								
$\bar{m}_{b,c}$	0.85	0.024	0.85	0.026	5.0	2.2	5.5	3.2
\bar{m}_s	0.58	0.058	0.13	0.025	1.62	1.57	1.66	0.67
α_s	5.60	0.19	5.64	0.21	7.9	4.7	7.86	6.70
$\langle \bar{q}q \rangle$	0.63	0.004	0.43	0.006	6.4	0.58	3.7	0.33
κ	1.88	1.11	4.86	1.05	28.3	21.5	12.9	29.1
$\langle \alpha_s G^2 \rangle$	0.63	0.010	0.48	0.008	3.35	1.0	1.43	0.74
M_0^2	1.95	0.056	1.43	0.054	4.1	3.43	1.65	3.06
$\langle \bar{q}q \rangle^2$	4.4	1.48	2.96	1.45	51	29.6	30.6	37.4
$\langle g^3 G^3 \rangle$	0.0	0.0	0.0	0.0	0.0	0.0	0.0	0.0
$d \geq 7$	1.0	1.4	2.0	1.49	11.0	25.4	10.0	23.3
<i>Total errors</i>	17.4	2.36	16.1	2.37	68.0	46.5	47.0	55.0

Fig. 28. **a)** M_{S_b} at LO as function of τ for a given value of $t_c = 48 \text{ GeV}^2$, $\mu = 4.5 \text{ GeV}$, mixing of currents $k = 0$ and for the QCD parameters in Table 2 and 3; The OPE is truncated at $d = 6$. We compare the effect of the on-shell or pole mass $M_b = 4.66 \text{ GeV}$ and of the running mass $\bar{m}_b(\bar{m}_b) = 4.18 \text{ GeV}$; **b)** The same as a) but for the coupling f_{S_b} .Fig. 29. **a)** M_{S_b} as function of τ for different truncation of the PT series at a given value of $t_c=48 \text{ GeV}^2$, $\mu = 4.5 \text{ GeV}$ and for the QCD parameters in Tables 2 and 3; **b)** The same as a) but for the coupling f_{S_b} .

14.5. Comparison of the LO results with the previous ones

• We also compare our QCD expression of the spectral function with the ones in^{16–18} where all authors use the four-quark current :

$$J_{4q} = (s^T \gamma_5 C u)(\bar{b} \gamma_5 C \bar{d}^T) , \quad (58)$$

which corresponds to the optimal choice $k = 0$, while, equivalently, we take the longitudinal part of the correlator associated to the current defined in Table 1:

– We do not agree with the QCD expression given in Ref.¹⁵ (see footnote on page 18).

– We agree with the perturbative and $\langle \alpha_s G^2 \rangle$ coefficient of,¹⁷ while the coefficient of their $\langle \bar{q}q \rangle$ is higher than ours by about a factor 1.3. We differs with¹⁷ for the four-quark condensate $\langle \bar{q}q \rangle^2$ coefficient which is about a factor 3 smaller in absolute value than the one of.¹⁶

– Ref.¹⁸ does not provide the expressions of his spectral function such that no comparison can be done.

• Hopefully, such discrepancies will affect only slightly the numerical analysis below because the contributions of the condensates are small though necessary corrections in the OPE.

• One can compare our numerical results with the ones in^{16–18} where the running mass $\bar{m}_b(m_b) \simeq (4.18 \sim 4.24)$ GeV has been implicitly used in different papers:

- The authors in Ref.¹⁶ choose $\tau \simeq (0.33 \sim 0.45)$ GeV^{−2}, $t_c \simeq (35 \sim 37)$ GeV², $\bar{m}_b(\bar{m}_b) \simeq 4.24$ GeV and found $M_{S_b} = (5.58 \pm 0.17)$ GeV.
- The authors in Ref.¹⁷ take $\tau \simeq (0.14 \sim 0.17)$ GeV^{−2}, $t_c \simeq 34$ GeV², $\bar{m}_b(\bar{m}_b) = 4.18$ GeV and obtain : $M_{S_b} = (5.58 \pm 0.14)$ GeV.
- The author in Ref.¹⁸ uses $\tau \simeq (0.20 \sim 0.22)$ GeV^{−2}, $t_c \simeq 37$ GeV², $\bar{m}_b(\bar{m}_b) = 4.18$ GeV and predicts : $M_{S_b} = (5.57 \pm 0.12)$ GeV and $f_{S_b} = 6.9$ keV.

• Using the previous values of the set $(\tau, t_c, \bar{m}_b(\bar{m}_b))$ choosen by previous authors, and our set of QCD parameters in Table 2, we deduce from Fig. 26:

- $M_{S_b} = (5.32 \sim 5.46)$ GeV (Ref.¹⁶ choice) ,
- $M_{S_b} = (5.46 \sim 5.47)$ GeV (Ref.¹⁷ choice) ,
- $M_{S_b} = (5.54 \sim 5.57)$ GeV (Ref.¹⁸ choice) ,

which agrees within the errors with the previous results.

• However, one should note that in the low-value of τ outside the stability regions used by different authors, the mass and the coupling are very sensitive to the value of the continuum threshold t_c as can be inspected from Fig. 26. In addition, the value of the mass is also affected by the change of τ ⁱ such that these predictions become unreliable.

ⁱLike in,¹⁴ the apparent stability shown in the figures of^{16–18} is only due to the choosen scale of the frame and to the small range of variation of τ or equivalently M^2 .

14.6. Improvement of the LO results including HO corrections

- We improve the previous LO results by including higher order (HO) perturbative corrections. In so doing, we assume that these corrections are dominated by the one from factorized diagrams (leading order in $1/N_c$ -expansion where N_c is the colour number). This assumption can be supported by the analysis of the $(\bar{b}d)(\bar{d}b)$ four-quark correlator controlling the $\bar{B}^0 B^0$ mixing by⁴⁷ where it has been shown that the non-factorizable diagram gives a small α_s -correction of about 10% of the factorizable one. Within this assumption, we proceed like in the case of the molecule by using the four-quark correlator as a convolution of two correlator built from bilinear quark anti-quark fields after Fierz transformations.

- We show the effects of these PT corrections in Fig. 29 for $\mu = 4.5$ GeV and $t_c = 48$ GeV², where one can notice that these corrections are small.

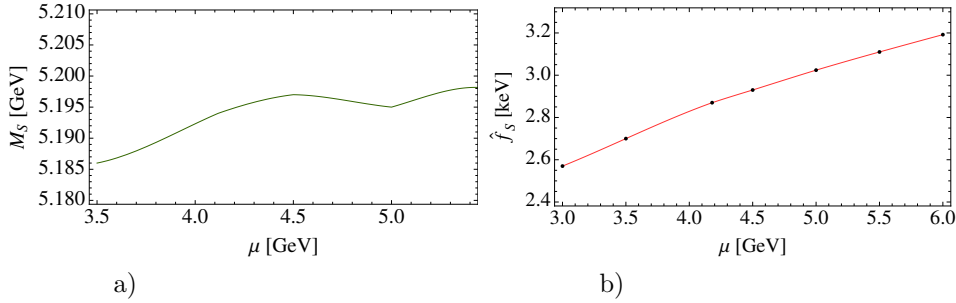


Fig. 30. **a)** M_{S_b} at NLO as function of μ , for the corresponding τ -stability region, for $t_c \simeq 48$ GeV² and for the QCD parameters in Tables 2 and 3; **b)** The same as a) but for the renormalization group invariant coupling \hat{f}_{S_b} .

14.7. μ -subtraction point stability

We show in Fig. 30 the dependence of M_{S_b} and of the renormalization group invariant coupling \hat{f}_{S_b} obtained at NLO of PT series on the choice of the subtraction constant μ . We consider as an optimal values the ones obtained for $\mu \simeq (4.5 \sim 5)$ GeV where we have a plateau for the mass and a slight inflexion point for \hat{f}_{S_b} . We deduce:

$$M_{S_b}^{NLO}(4.5) \simeq (5197 \sim 5195) \text{ MeV} ,$$

$$\hat{f}_{S_b}^{NLO} \simeq (2.93 \sim 3.02) \text{ keV} \implies f_{S_b}^{NLO}(4.5) \simeq (9.38 \sim 10.06) \text{ keV} (59)$$

14.8. Error induced by the truncation of the OPE

We show in Fig. 31 the effect of a class of $d = 7$ condensates for different values of the factorization violation parameter χ . Our estimate of the error induced by the truncation of the OPE corresponds to the choice $\chi = 4$.

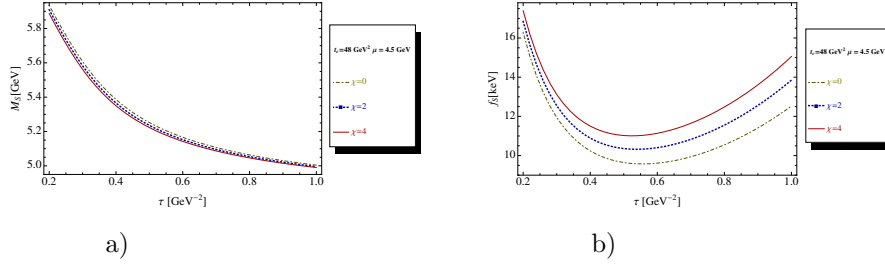
32 *R.M. Albuquerque et al.*

Fig. 31. **a)** M_{S_b} as function of τ , for different values of the $d = 7$ condensate contribution (χ measures the violation of factorization), at a given value of $t_c = 48 \text{ GeV}^2$, $\mu = 4.5 \text{ GeV}$ and for the QCD parameters in Tables 2 and 3; **b)** The same as a) but for the coupling f_{S_b} .

14.9. Final results

We conclude from previous analysis that the mass and coupling of the 0^+ scalar four-quark state to N2LO is:

$$M_{S_b} \simeq (5196 \pm 17) \text{ MeV} ,$$

$$\hat{f}_{S_b} \simeq (2.98 \pm 0.70) \text{ keV} \quad \implies \quad f_{S_b}(4.5) \simeq (9.99 \pm 2.36) \text{ keV} , \quad (60)$$

where the errors come from Table 5. Our mass prediction is lower than previous sum rule results^{16–18} and the $D0$ candidate $X(5568)$.

15. Spectral function of the axial-vector four-quark $(su)(\bar{b}\bar{d})$ state

The expression of the axial-vector spectral function comes from the transverse part of the corresponding correlator built from the 1^+ current. It reads:

$$\rho^{pert} = \frac{(1+k^2)M_b^8}{5 \cdot 3 \cdot 2^{13} \pi^6} \left[\frac{5}{x^4} - \frac{96}{x^3} - \frac{945}{x^2} + \frac{480}{x} - 60 \left(\frac{9}{x^2} + \frac{16}{x} + 3 \right) \text{Log}(x) + 555 + x^2 \right] ,$$

$$\rho^{\langle \bar{q}q \rangle} = -\frac{(1-k^2)M_b^5}{3 \cdot 2^6 \pi^4} \langle \bar{q}q \rangle \left[\frac{1}{x^2} + \frac{9}{x} + 6 \left(\frac{1}{x} + 1 \right) \text{Log}(x) - 9 - x \right]$$

$$- \frac{m_s M_b^4}{3 \cdot 2^9 \pi^4} \langle \bar{q}q \rangle \left[2(1-k^2) - (1+k^2)\kappa \right] \left(\frac{3}{x^2} - \frac{16}{x} - 12 \text{Log}(x) + 12 + x^2 \right) ,$$

$$\rho^{\langle G^2 \rangle} = -\frac{(1+k^2)m_b^4}{3^3 \cdot 2^{13} \pi^6} 4\pi \langle \alpha_s G^2 \rangle \left[\frac{3}{x^2} + \frac{212}{x} + 48 \left(\frac{2}{x} + 3 \right) \text{Log}(x) - 198 - 12x - 5x^2 \right] ,$$

$$\rho^{\langle \bar{q}Gq \rangle} = \frac{(1-k^2)M_b^3}{2^7 \pi^4} \langle \bar{q}Gq \rangle \left(\frac{1}{x} + 2 \text{Log}(x) - x \right)$$

$$+ \frac{m_s M_b^2}{3^2 \cdot 2^8 \pi^4} \langle \bar{q}Gq \rangle \left[6(1-k^2) + (1+k^2)\kappa \right] \left(\frac{2}{x} - 3 + x^2 \right) ,$$

$$\begin{aligned}\rho^{\langle\bar{q}q\rangle^2} &= \frac{(1-k^2)M_b^2}{3^2 2^3 \pi^2} \rho^{\langle\bar{q}q\rangle^2} \kappa \left(\frac{2}{x} - 3 + x^2 \right) \\ &\quad + \frac{m_s M_b}{3 2^3 \pi^2} \rho^{\langle\bar{q}q\rangle^2} \left[2(1+k^2) - (1-k^2)\kappa \right] (1-x), \\ \rho^{\langle G^3 \rangle} &= \frac{(1+k^2)M_b^2}{3^3 2^{15} \pi^6} \langle g_s^3 G^3 \rangle \left[\frac{9}{x^2} - \frac{160}{x} - 12 \left(\frac{4}{x} + 9 \right) \text{Log}(x) + 144 + 7x^2 \right].\end{aligned}\quad (61)$$

The contribution of a class of $d = 7$ condensate for $m_s = 0$ is:

$$\rho^{\langle\bar{q}q\rangle\langle G^2 \rangle} = -(1-k^2) \frac{M_b \langle\bar{q}q\rangle}{3^2 2^8 \pi^4} 4\pi \langle\alpha_s G^2\rangle \left(\frac{2}{x} + 6 \text{Log } x + 7 - 9x \right). \quad (62)$$

16. Mass and coupling of the 1^+ axial-vector four-quark state

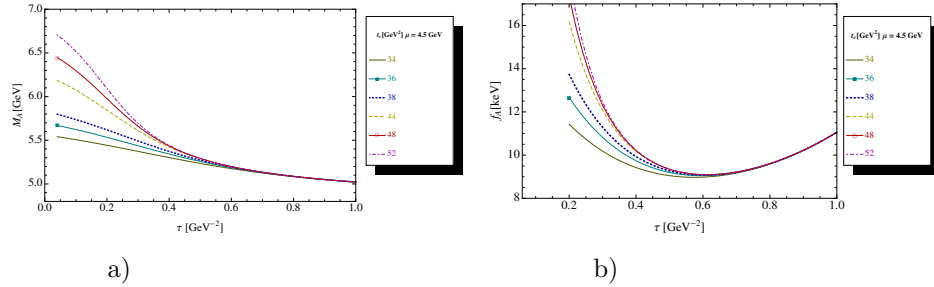


Fig. 32. **a)** M_{A_b} at LO as function of τ and different values of t_c . We use $\mu = 4.5$ GeV, the mixing parameter $k = 0$ and the QCD parameters in Tables 2 and 3; **b)** The same as a) but for the coupling f_{A_b} .

The analysis is similar to the one in previous sections. The curves have the same

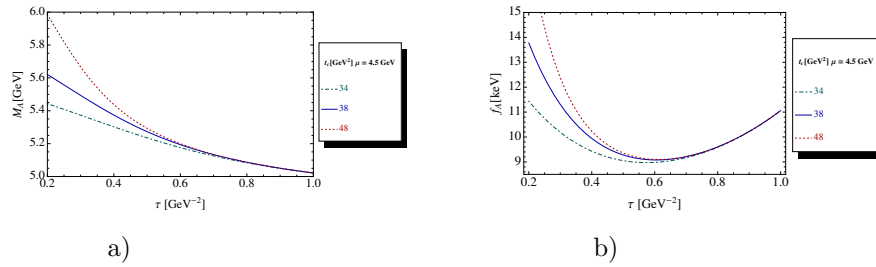


Fig. 33. The same as Fig. 32 but for NLO.

feature as the one of the 0^+ scalar state. The optimal choice of the interpolating current is also obtained for $k = 0$.

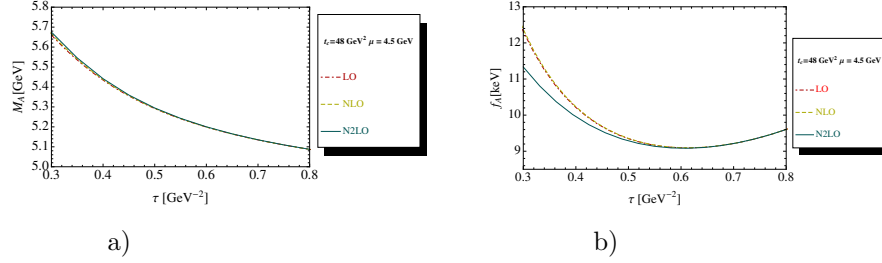
34 *R.M. Albuquerque et al.*


Fig. 34. **a)** M_{A_b} as function of τ for different truncation of the PT series at a given value of $t_c=48$ GeV^2 , $\mu = 4.5$ GeV and for the QCD parameters in Tables 2 and 3; **b)** The same as a) but for the coupling f_{A_b} .

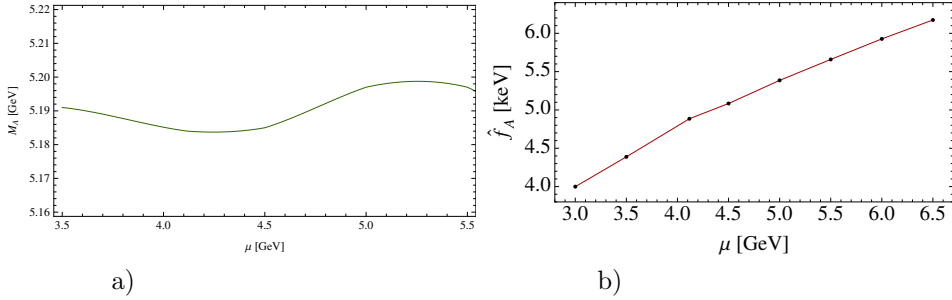


Fig. 35. **a)** M_{A_b} at NLO as function of μ , for the corresponding τ -stability region, for $t_c \simeq 48$ GeV^2 and for the QCD parameters in Tables 2 and 3; **b)** The same as a) but for the renormalization group invariant coupling \hat{f}_{A_b} .

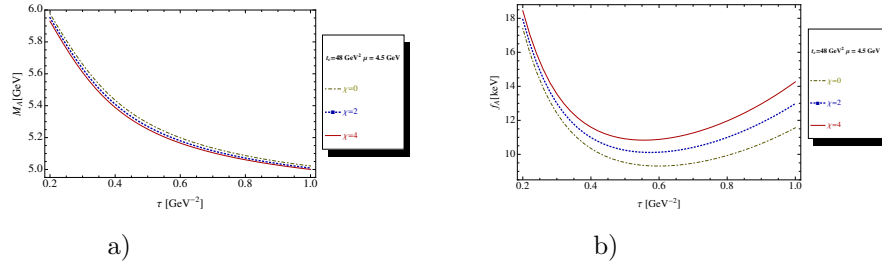


Fig. 36. **a)** M_{A_b} as function of τ , for different values of the $d = 7$ condensate contribution (χ measures the violation of factorization), at a given value of $t_c=48$ GeV^2 , $\mu = 4.5$ GeV and for the QCD parameters in Tables 2 and 3; **b)** The same as a) but for the coupling f_{A_b} .

16.1. τ - and t_c -stabilities

- We show in Fig. 32 the τ -behaviour of the mass and coupling at LO for different t_c and for $\mu=4.5$ GeV .

16.2. NLO result and HO PT corrections

The NLO result is shown in Fig. 33 and a comparison of the effects of PT corrections is shown in Fig. 34. We have τ -stability for $\tau \simeq (0.52 \sim 0.56) \text{ GeV}^{-2}$ while the corresponding range of t_c values is from 34 to 48 GeV^2 .

16.3. μ - subtraction point stability at NLO

We study the effect of the subtraction point in Fig. 35 where we have stability for $\mu \simeq 4.5 \text{ GeV}$.

16.4. Error induced by the truncation of the OPE

We show in Fig. 36 the effect of a class of $d = 7$ condensates for different values of the factorization violation parameter χ . Our estimate of the error induced by the truncation of the OPE corresponds to the choice $\chi = 4$.

16.5. Final results

From previous analysis, we deduce the final results to N2LO:

$$\begin{aligned} M_{A_b} &\simeq (5186 \pm 16) \text{ MeV} , \\ \hat{f}_{A_b} &\simeq (5.05 \pm 1.32) \text{ keV} \quad \Longrightarrow \quad f_{A_b} \simeq (9.04 \pm 2.37) \text{ keV} , \end{aligned} \quad (63)$$

where the errors come from the quadratic sum of the ones in Table 5.

17. Extension of the analysis to the charm quark

One can naturally extend the previous analysis done in the b -quark channel to the charm quark. In so doing, we replace the b -quark mass by the c -quark one, use $n_f = 4$ and the QCD parameters in Tables 2 and 3.

17.1. 0^+ scalar DK molecule

- The analysis is very similar to the previous one which we illustrate for the case of a scalar DK molecule. In Fig. 37, we show the τ -behaviour of the mass and coupling to lowest order (LO) for different values of t_c , for $\mu = 2 \text{ GeV}$ and for the input parameters in Tables 2 and 3. One can see a τ -stability of about 0.6 GeV^{-2} starting from $t_c = 12 \text{ GeV}^2$ while t_c -stability is reached from $t_c = 18 \text{ GeV}^2$. At lowest order, one obtains for $\mu=2 \text{ GeV}$:

$$M_{DK}^{LO} \simeq (2395 \sim 2397) \text{ MeV} \quad \text{and} \quad f_{DK}^{LO} \simeq (250 \sim 254) \text{ keV} . \quad (64)$$

- The analysis of the μ -behaviour in Fig. 39 indicates a μ -stability for $\mu = 2 \text{ GeV}$.

- The effects of the truncation of the PT series are shown in Fig. 40. One can notice that the PT corrections are small both for the coupling and for the mass

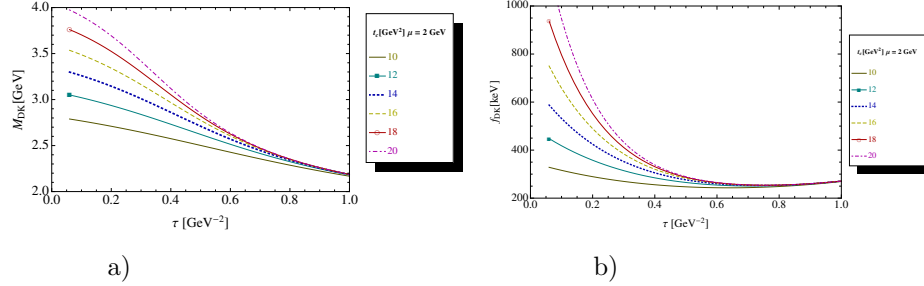
36 *R.M. Albuquerque et al.*


Fig. 37. **a)** M_{DK} at LO as function of τ and different values of t_c . We use $\mu = 2$ GeV, the mixing parameter $k = 0$ and the QCD parameters in Tables 2 and 3; **b)** The same as a) but for the coupling f_{DK} .

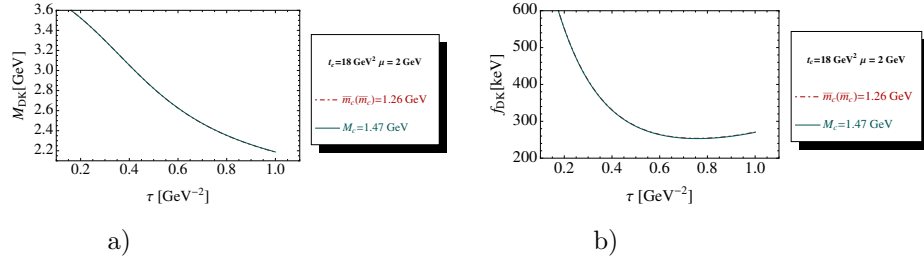


Fig. 38. **a)** M_{DK} at LO as function of τ for a given value of $t_c = 18$ GeV², $\mu = 2$ GeV, mixing of currents $k = 0$ and for the QCD parameters in Tables 2 and 3. The OPE is truncated at $d = 6$. We compare the effect of the on-shell or pole mass $M_c = 1.47$ GeV and of the running mass $\bar{m}_c(\bar{m}_c) = 1.26$ GeV; **b)** The same as a) but for the coupling f_{DK} .

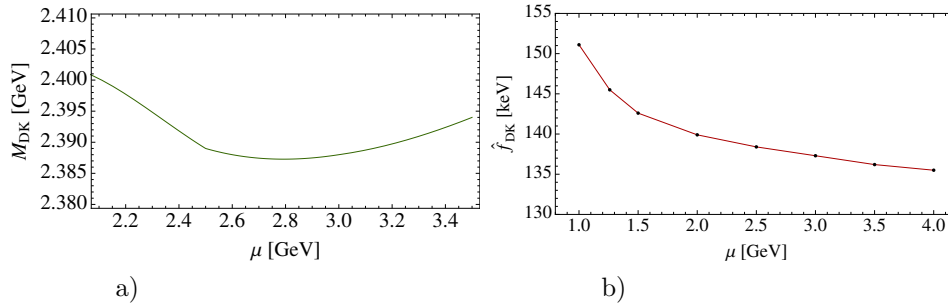


Fig. 39. **a)** M_{DK} at NLO as function of μ , for the corresponding τ -stability region, for $t_c \simeq 18$ GeV² and for the QCD parameters in Tables 2 and 3. **b)** The same as a) but for the renormalization group invariant coupling \hat{f}_{DK} .

which justify the LO result and the (a priori) use of the running heavy quark mass. It also shows that the effect of the tachyonic gluon mass is small by duality with HO corrections.

- The convergence of the OPE is tested in Fig. 41 by adding the contribution of

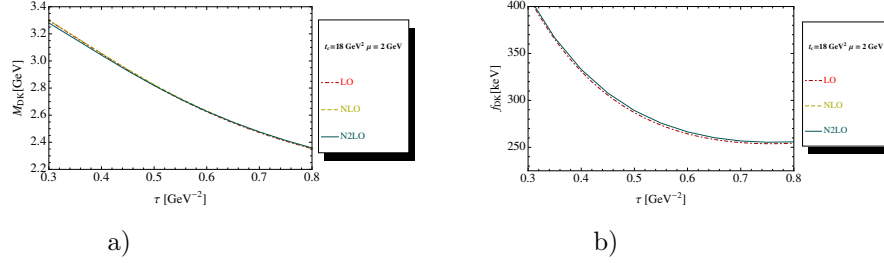


Fig. 40. **a)** M_{DK} as function of τ for different truncation of the PT series at a given value of $t_c=18$ GeV^2 , $\mu = 2$ GeV and for the QCD parameters in Tables 2 and 3; **b)** The same as a) but for the coupling f_{DK} .

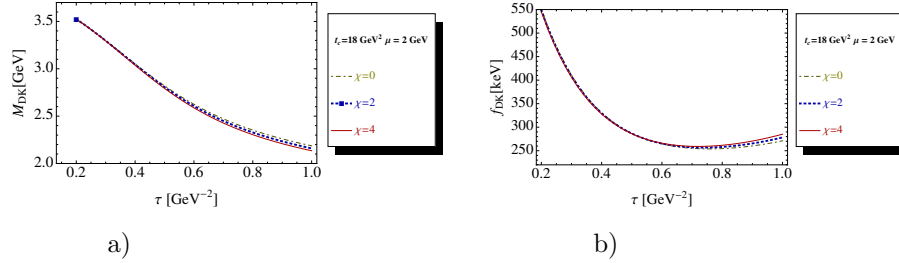


Fig. 41. **a)** M_{DK} as function of τ , for different values of the $d = 7$ condensate contribution (χ measures the violation of factorization), at a given value of $t_c=18$ GeV^2 , $\mu = 2$ GeV and for the QCD parameters in Tables 2 and 3; **b)** The same as a) but for the coupling f_{DK} .

Table 6. Different sources of errors for the estimate of the molecule masses (in units of MeV) and couplings (in units of keV) in the c -quark channel.

Inputs [GeV] ^d	ΔM_{D^*K}	Δf_{D^*K}	ΔM_{DK}	Δf_{DK}	$\Delta M_{D_s^*\pi}$	$\Delta f_{D_s^*\pi}$	$\Delta M_{D_s\pi}$	$\Delta f_{D_s\pi}$
<i>LSR parameters</i>								
$t_c = (12 \sim 18)$	2	1.5	0.0	1.5	8.5	2.5	2.5	2
$\mu = (2.0 \sim 2.5)$	9	13.5	5	15.5	4	14.5	4.5	17
$\tau = \tau_{min} \pm 0.02$	24	0.17	24	0.10	30	0.12	23.2	0.06
<i>QCD inputs</i>								
\bar{m}_c	5.4	2.8	5.5	6.7	5.0	3.32	5.58	3.58
\bar{m}_s	0.13	0.55	0.13	0.48	0.85	0.76	1.0	0.63
α_s	7.9	5.8	8.1	6.68	9.0	6.55	7.92	7.32
$\langle \bar{q}q \rangle$	3.7	0.24	3.4	0.51	1.58	0.16	0.36	0.36
κ	11.4	22.5	13.5	27.9	6.83	0.7	8.10	1.58
$\langle \alpha_s G^2 \rangle$	2.1	1.3	4.7	1.95	2.16	1.13	0.60	1.83
M_0^2	2.3	2.8	1.60	1.38	0.90	1.28	0.60	0.47
$\langle \bar{q}q \rangle^2$	32.1	32.5	29.4	34.9	34	37.37	23.05	41.23
$\langle g^3 G^3 \rangle$	0	0	0.0	0.0	0.0	0.0	0.0	0.0
$d \geq 7$	3	31.4	1	4.7	3.5	27.6	7	2
<i>Total errors</i>	48.1	52.4	42	48	48.1	49.4	36.7	46

the $d = 7$ condensate. It induces an error:

$$\Delta f_{DK}^{OPE} \simeq \pm 4.7 \text{ keV} , \quad \Delta M_{DK}^{OPE} \simeq \pm 1 \text{ MeV} . \quad (65)$$

• From the previous analysis, we deduce the final result including N2LO PT perturbative $\oplus d \leq 6$ dimension contributions taking $t_c \simeq 12 \sim 18$ GeV^2 and

38 *R.M. Albuquerque et al.*

$\mu=2$ GeV:

$$\begin{aligned} M_{DK} &\simeq (2402 \pm 42) \text{ MeV} , \\ \hat{f}_{DK} &\simeq (139 \pm 26) \text{ keV} \quad \Rightarrow \quad f_{DK} \simeq (254 \pm 48) \text{ keV} , \end{aligned} \quad (66)$$

where the different sources of errors come from Table 6.

17.2. 1^+ axial-vector D^*K molecule

• The analysis of the 1^+ D^*K molecule exhibits the same feature as the one of the DK molecule. We show the results of the analysis in Figs 42 to 46. The optimal result is obtained for $\mu \simeq 2$ GeV:

$$\begin{aligned} M_{D^*K} &\simeq (2395 \pm 48) \text{ MeV} , \\ \hat{f}_{D^*K} &\simeq (155 \pm 36) \text{ keV} \quad \Rightarrow \quad f_{D^*K} \simeq (226 \pm 52) \text{ keV} , \end{aligned} \quad (67)$$

where the different sources of errors come from Table 6.

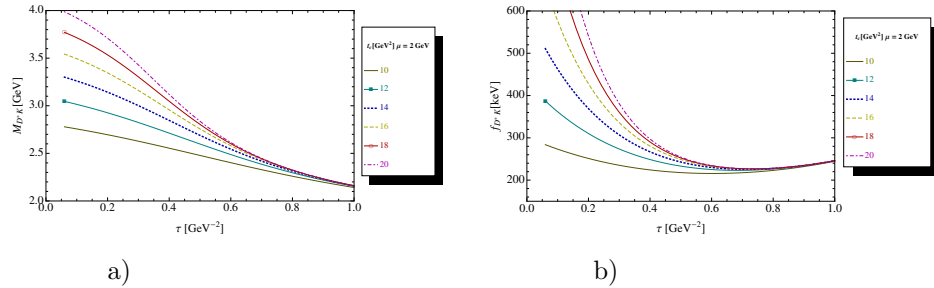


Fig. 42. **a)** M_{D^*K} at LO as function of τ and different values of t_c . We use $\mu = 2$ GeV, the mixing parameter $k = 0$ and the QCD parameters in Tables 2 and 3; **b)** The same as a) but for the coupling f_{D^*K} .

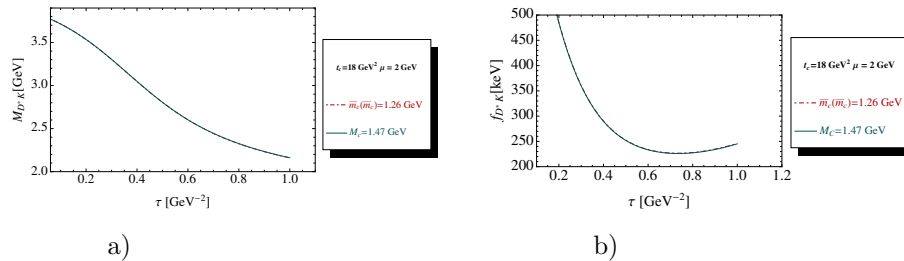


Fig. 43. **a)** M_{D^*K} at LO as function of τ for a given value of $t_c = 18 \text{ GeV}^2$, $\mu = 2$ GeV, mixing of currents $k = 0$ and for the QCD parameters in Tables 2 and 3. The OPE is truncated at $d = 6$. We compare the effect of the on-shell or pole mass $M_c = 1.47 \text{ GeV}$ and of the running mass $\bar{m}_c(\bar{m}_c) = 1.26 \text{ GeV}$; **b)** The same as a) but for the coupling f_{D^*K} .

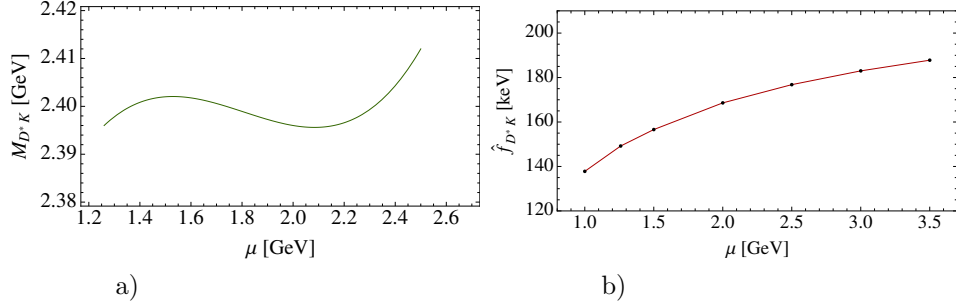


Fig. 44. **a)** M_{D^*K} at NLO as function of μ , for the corresponding τ -stability region, for $t_c \simeq 18 \text{ GeV}^2$ and for the QCD parameters in Tables 2 and 3; **b)** The same as a) but for the renormalization group invariant coupling \hat{f}_{D^*K} .

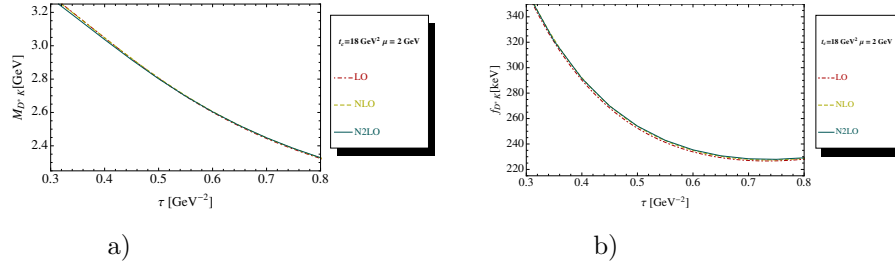


Fig. 45. **a)** M_{D^*K} as function of τ for different truncation of the PT series at a given value of $t_c=18 \text{ GeV}^2$, $\mu = 2 \text{ GeV}$ and for the QCD parameters in Tables 2 and 3; **b)** The same as a) but for the coupling f_{D^*K} .

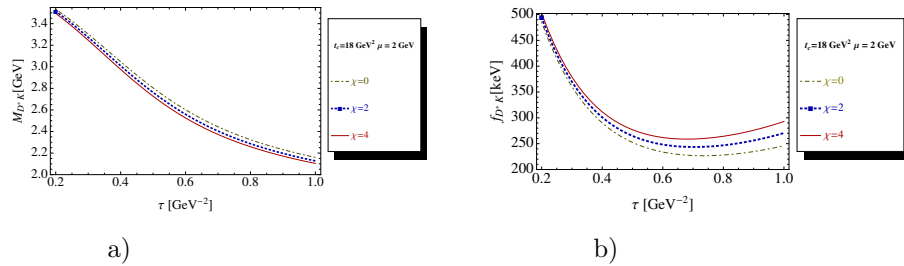


Fig. 46. **a)** M_{D^*K} as function of τ , for different values of the $d = 7$ condensate contribution (χ measures the violation of factorization), at a given value of $t_c=18 \text{ GeV}^2$, $\mu = 2 \text{ GeV}$ and for the QCD parameters in Tables 2 and 3; **b)** The same as a) but for the coupling f_{D^*K} .

17.3. 1^+ axial- vector $D_s^*\pi$ molecule

• The analysis is similar to the previous ones. We show the results of the analysis in Figs 47 to 51. Here, the optimal result is obtained for $\mu \simeq 2.5 \text{ GeV}$. Using the

40 *R.M. Albuquerque et al.*

errors quoted in Table 6, we deduce at N2LO:

$$\begin{aligned} M_{D_s^* \pi} &\simeq (2395 \pm 48) \text{ MeV} , \\ \hat{f}_{D_s^* \pi} &\simeq (215 \pm 35) \text{ keV} \quad \Rightarrow \quad f_{D_s^* \pi} \simeq (308 \pm 49) \text{ keV} , \end{aligned} \quad (68)$$

where the different sources of errors come from Table 6.

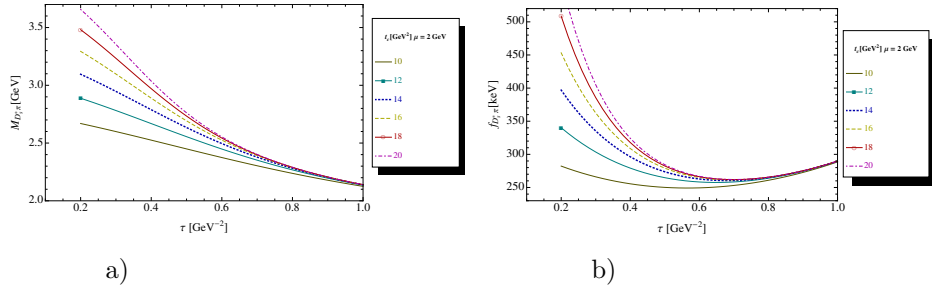


Fig. 47. **a)** $M_{D_s^* \pi}$ at LO as function of τ and different values of t_c . We use $\mu = 2 \text{ GeV}$, the mixing parameter $k = 0$ and the QCD parameters in Tables 2 and 3; **b)** The same as a) but for the coupling $f_{D_s^* \pi}$.

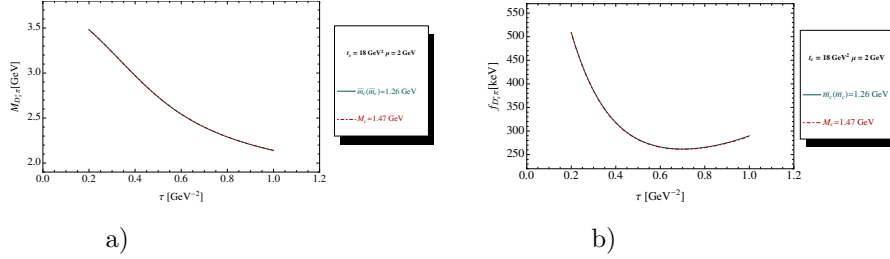


Fig. 48. **a)** $M_{D_s^* \pi}$ at LO as function of τ for a given value of $t_c = 18 \text{ GeV}^2$, $\mu = 2 \text{ GeV}$ and for the QCD parameters in Tables 2 and 3. The OPE is truncated at $d = 6$. We compare the effect of the on-shell or pole mass $M_c = 1.47 \text{ GeV}$ and of the running mass $\bar{m}_c(\bar{m}_c) = 1.26 \text{ GeV}$; **b)** The same as a) but for the coupling $f_{D_s^* \pi}$.

17.4. 0^+ scalar $D_s \pi$ molecule

• The analysis is similar to the previous ones. We show the results of the analysis in Figs 52 to 56. Using the error quoted in Table 4, we deduce at N2LO and for $\mu = 2.5 \text{ GeV}$:

$$\begin{aligned} M_{D_s \pi} &\simeq (2404 \pm 37) \text{ MeV} , \\ \hat{f}_{D_s \pi} &\simeq (160 \pm 22) \text{ keV} \quad \Rightarrow \quad f_{D_s \pi} \simeq (331 \pm 46) \text{ keV} , \end{aligned} \quad (69)$$

where the different sources of errors come from Table 6.

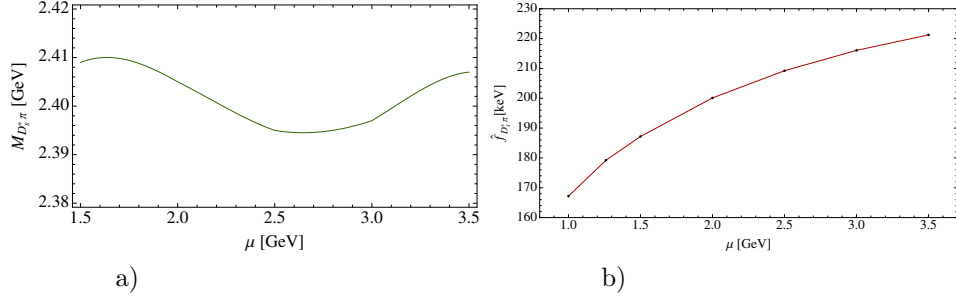


Fig. 49. **a)** $M_{D_s^* \pi}$ at NLO as function of μ , for the corresponding τ -stability region, for $t_c \simeq 18 \text{ GeV}^2$ and for the QCD parameters in Tables 2 and 3; **b)** The same as a) but for the renormalization group invariant coupling $\hat{f}_{D_s^* \pi}$.

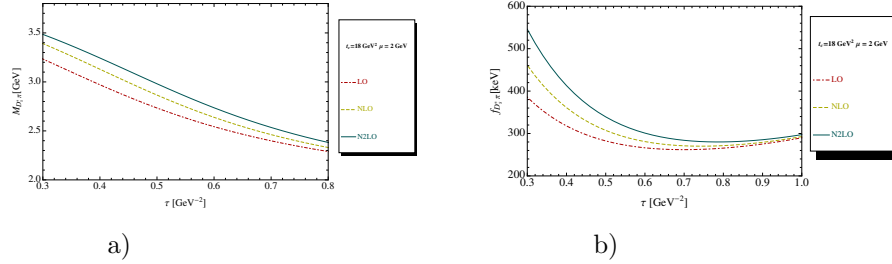


Fig. 50. **a)** $M_{D_s^* \pi}$ as function of τ for different truncation of the PT series at a given value of $t_c=18 \text{ GeV}^2$, $\mu = 2 \text{ GeV}$ and for the QCD parameters in Tables 2 and 3; **b)** The same as a) but for the coupling $f_{D_s^* \pi}$.

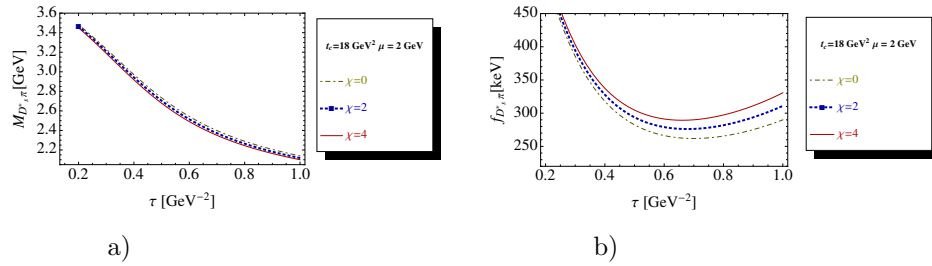


Fig. 51. **a)** $M_{D_s^* \pi}$ as function of τ , for different values of the $d = 7$ condensate contribution (χ measures the violation of factorization), at a given value of $t_c=18 \text{ GeV}^2$, $\mu = 2 \text{ GeV}$ and for the QCD parameters in Tables 2 and 3; **b)** The same as a) but for the coupling $f_{D_s^* \pi}$.

17.5. 0^+ scalar four-quark state

• The analysis is very similar to the previous one. In Fig. 57, we show the τ -behaviour of the mass and coupling at lowest order (LO) for different values of t_c , for $\mu = 2 \text{ GeV}$ and for the input parameters in Tables 2 and 3. One can see a τ -stability of about 0.6 GeV^{-2} starting from $t_c = 12 \text{ GeV}^2$ while t_c -stability is

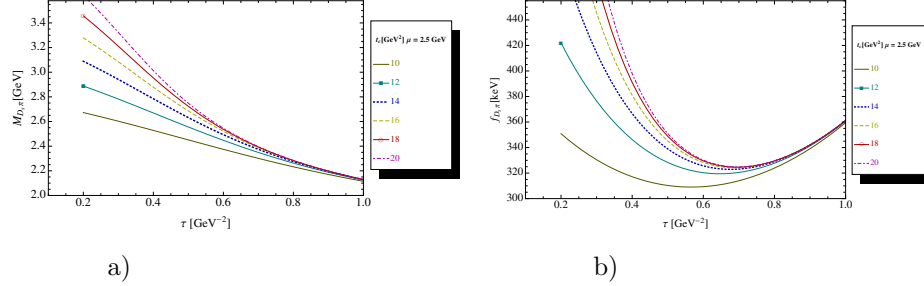
42 *R.M. Albuquerque et al.*


Fig. 52. **a)** $M_{D_s\pi}$ at LO as function of τ and different values of t_c . We use $\mu = 2.5$ GeV, the mixing parameter $k = 0$ and the QCD parameters in Tables 2 and 3; **b)** The same as a) but for the coupling $f_{D_s\pi}$.

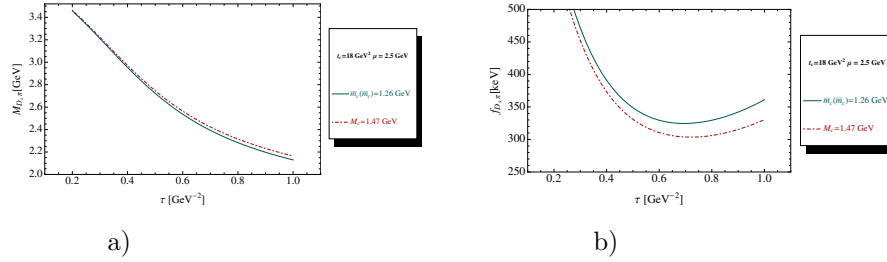


Fig. 53. **a)** $M_{D_s\pi}$ at LO as function of τ for a given value of $t_c = 18 \text{ GeV}^2$, $\mu = 2.5 \text{ GeV}$, mixing of currents $k = 0$ and for the QCD parameters in Tables 2 and 3. The OPE is truncated at $d = 6$. We compare the effect of the on-shell or pole mass $M_c = 1.47 \text{ GeV}$ and of the running mass $\bar{m}_c(\bar{m}_c) = 1.26 \text{ GeV}$; **b)** The same as a) but for the coupling $f_{D_s\pi}$.

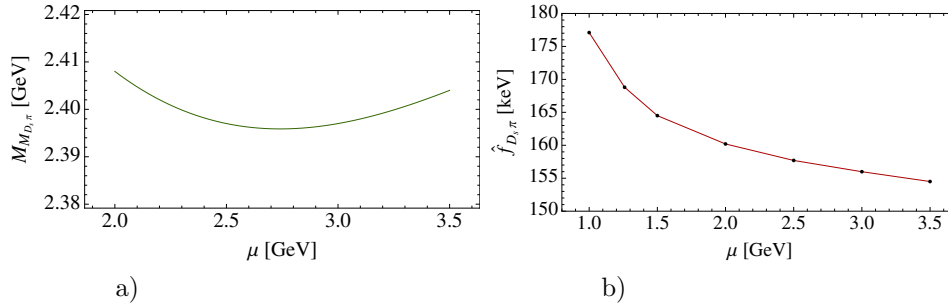


Fig. 54. **a)** $M_{D_s\pi}$ at LO as function of μ , for the corresponding τ -stability region, for $t_c \simeq 18 \text{ GeV}^2$ and for the QCD parameters in Tables 2 and 3; **b)** The same as a) but for the renormalization group invariant coupling $\hat{f}_{D_s\pi}$.

reached from $t_c = 18 \text{ GeV}^2$.

17.6. Error induced by the truncation of the OPE

We show in Fig. 61 the effect of a class of $d = 7$ condensates for different values of the factorization violation parameter χ . Our estimate of the error induced by the

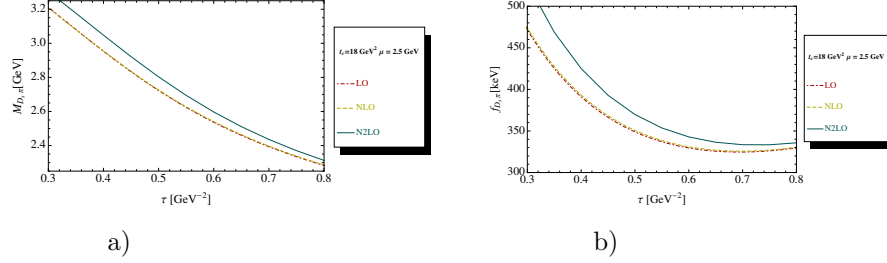


Fig. 55. **a)** $M_{D_s\pi}$ as function of τ for different truncation of the PT series at a given value of $t_c=18$ GeV^2 , $\mu = 2.5$ GeV and for the QCD parameters in Tables 2 and 3; **b)** The same as a) but for the coupling $f_{D_s\pi}$.

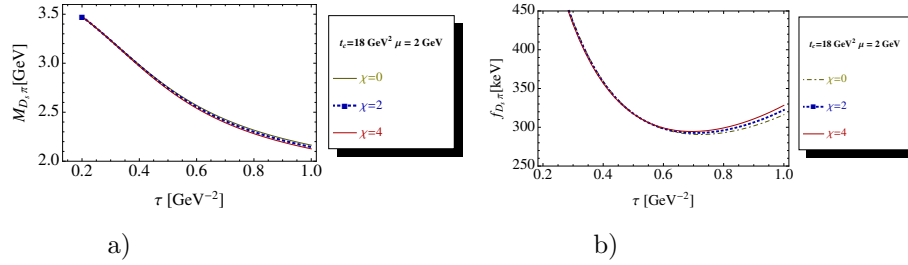


Fig. 56. **a)** $M_{D_s\pi}$ as function of τ , for different values of the $d = 7$ condensate contribution (χ measures the violation of factorization), at a given value of $t_c=18$ GeV^2 , $\mu = 2$ GeV and for the QCD parameters in Tables 2 and 3; **b)** The same as a) but for the coupling $f_{D_s\pi}$.

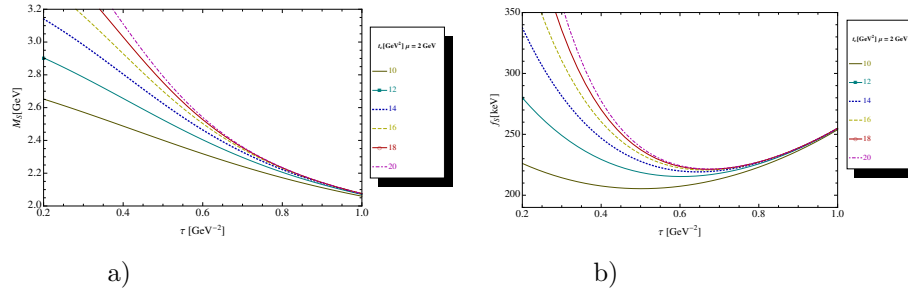


Fig. 57. **a)** M_{S_c} at LO as function of τ for $\mu = 2$ GeV , $t_c=18$ GeV^2 , mixing currents $k = 0$ and for the QCD parameters in Tables 2 and 3; **b)** The same as a) but for the coupling f_{S_c} .

truncation of the OPE corresponds to the choice $\chi = 4$. At lowest order, one obtains for $\mu=2$ GeV :

$$M_{S_c}^{LO} \simeq (2381 \sim 2386) \text{ MeV} \quad \text{and} \quad f_{S_c}^{LO} \simeq (215 \sim 221) \text{ keV} . \quad (70)$$

- The analysis of the μ -behaviour in Fig. 59 indicates a μ -stability for $\mu = 2$ GeV .
- The effects of the truncation of the PT series are shown in Fig. 60, where one can notice that the PT corrections are small both for the coupling and for the mass.
- From the previous analysis, we deduce the final result including N2LO PT

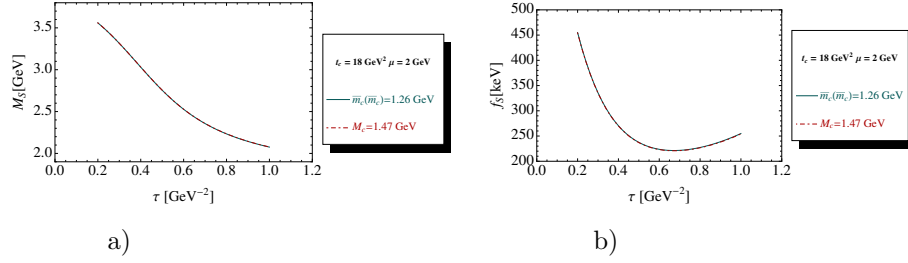
44 *R.M. Albuquerque et al.*


Fig. 58. **a)** M_{S_c} at LO as function of τ for a given value of $t_c = 18 \text{ GeV}^2$, $\mu = 2 \text{ GeV}$, mixing of currents $k = 0$ and for the QCD parameters in Tables 2 and 3; The OPE is truncated at $d = 6$. We compare the effect of the on-shell or pole mass $M_c = 1.47 \text{ GeV}$ and of the running mass $\bar{m}_c(\bar{m}_c) = 1.26 \text{ GeV}$; **b)** The same as a) but for the coupling f_{S_c} .

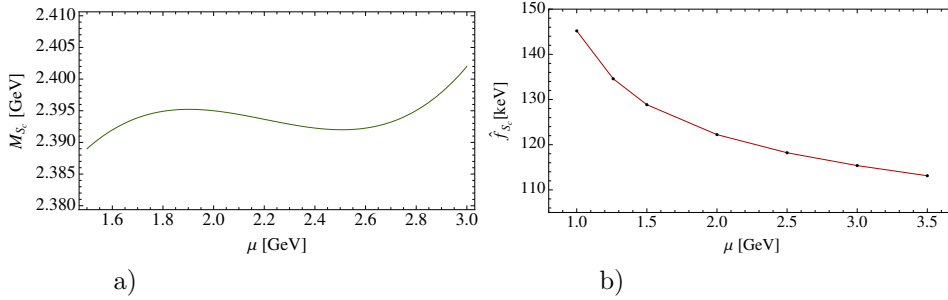


Fig. 59. **a)** M_{S_c} at NLO as function of μ , for the corresponding τ -stability region, for $t_c \simeq 18 \text{ GeV}^2$ and for the QCD parameters in Tables 2 and 3; **b)** The same as a) but for the renormalization group invariant coupling \hat{f}_{S_c} .

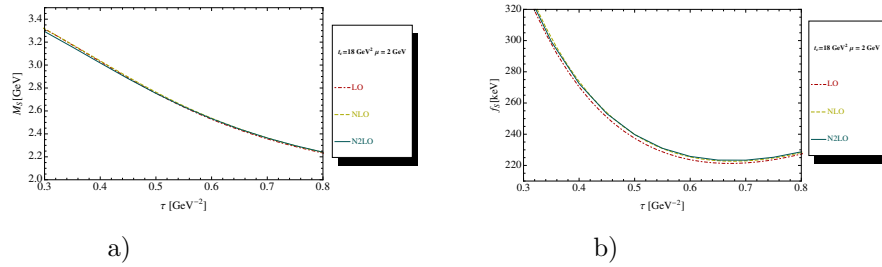


Fig. 60. **a)** M_{S_c} as function of τ for different truncation of the PT series at a given value of $t_c = 18 \text{ GeV}^2$, $\mu = 2 \text{ GeV}$ and for the QCD parameters in Tables 2 and 3; **b)** The same as a) but for the coupling f_{S_c} .

perturbative $\oplus d \leq 6$ dimension contributions. We take $t_c \simeq (12 \sim 18) \text{ GeV}^2$ and the optimal choice $\mu = 2 \text{ GeV}$:

$$\begin{aligned} M_{S_c} &\simeq (2395 \pm 68) \text{ MeV} , \\ \hat{f}_{S_c} &\simeq (122 \pm 26) \text{ keV} \implies f_{S_c} \simeq (221 \pm 47) \text{ keV} , \end{aligned} \quad (71)$$

where the different sources of errors come from Table 6.

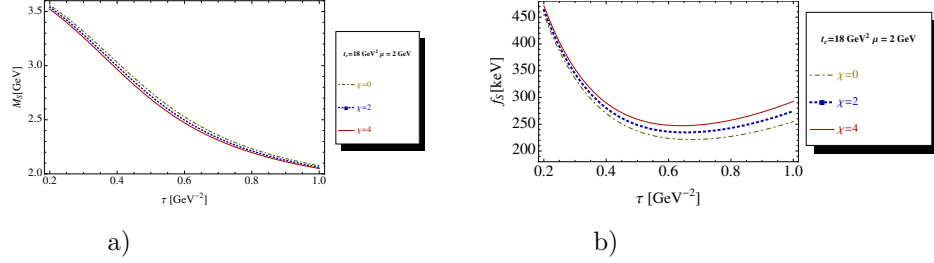


Fig. 61. **a)** M_{S_c} as function of τ , for different values of the $d = 7$ condensate contribution (χ measures the violation of factorization), at a given value of $t_c = 18 \text{ GeV}^2$, $\mu = 2 \text{ GeV}$ and for the QCD parameters in Tables 2 and 3; **b)** The same as a) but for the coupling f_{S_c} .

17.7. 1^+ axial-vector four-quark state

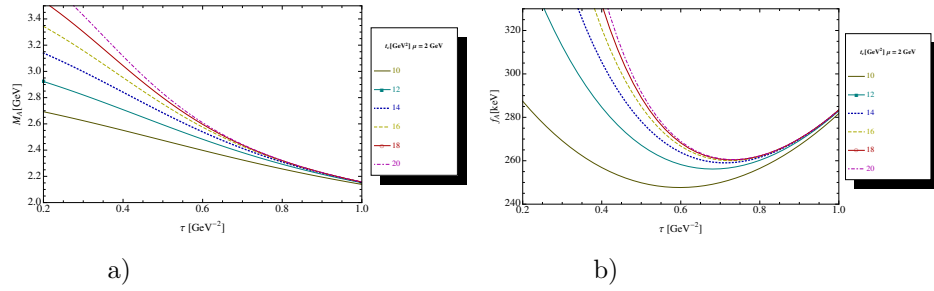


Fig. 62. **a)** M_{A_c} at LO as function of τ for $\mu = 2 \text{ GeV}$, $t_c = 18 \text{ GeV}^2$, mixing currents $k = 0$ and for the QCD parameters in Tables 2 and 3; **b)** The same as a) but for the coupling f_{A_c} .

We repeat the previous analysis for the 1^+ axial-vector four-quark state. In Fig. 62,

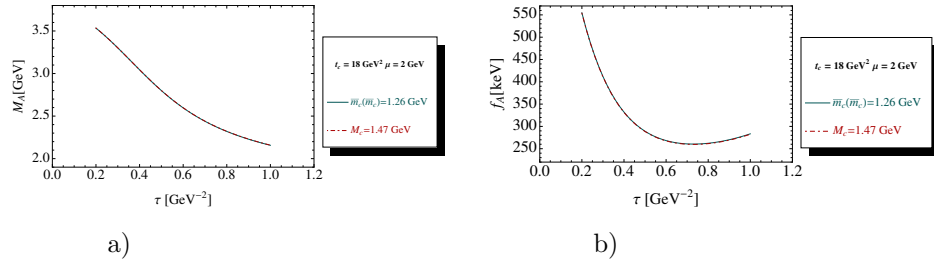


Fig. 63. **a)** M_{A_c} at LO as function of τ for a given value of $t_c = 18 \text{ GeV}^2$, $\mu = 2 \text{ GeV}$, mixing of currents $k = 0$ and for the QCD parameters in Tables 2 and 3. The OPE is truncated at $d = 6$. We compare the effect of the on-shell or pole mass $M_c = 1.47 \text{ GeV}$ and of the running mass $\bar{m}_c(\bar{m}_c) = 1.26 \text{ GeV}$; **b)** The same as a) but for the coupling f_{A_c} .

we show the τ -behaviour of the mass and coupling at lowest order (LO) for different values of t_c , for $\mu = 2 \text{ GeV}$ and for the input parameters in Tables 2 and 3. One can

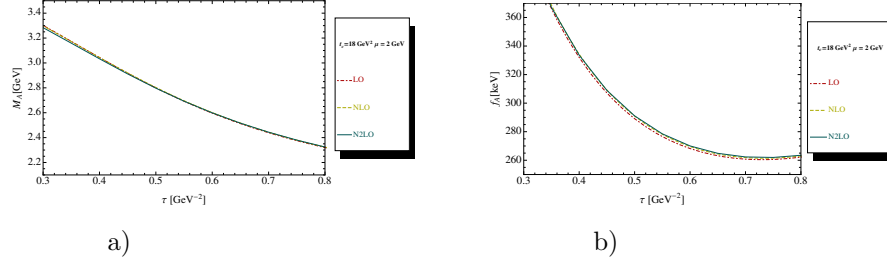


Fig. 64. **a)** M_{A_c} as function of τ for different truncation of the PT series at a given value of $t_c = 18 \text{ GeV}^2$, $\mu = 2 \text{ GeV}$ and for the QCD parameters in Tables 2 and 3. **b)** The same as a) but for the coupling f_{A_c} .

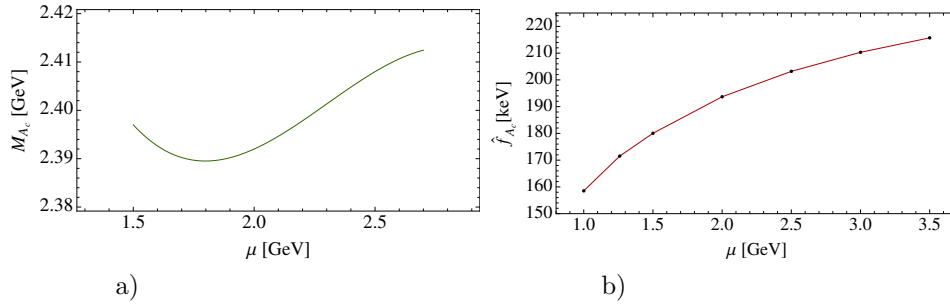


Fig. 65. **a)** M_{A_c} at NLO as function of μ , for the corresponding τ -stability region, for $t_c \simeq 18 \text{ GeV}^2$ and for the QCD parameters in Tables 2 and 3. **b)** The same as a) but for the renormalization group invariant coupling \hat{f}_{A_c} .

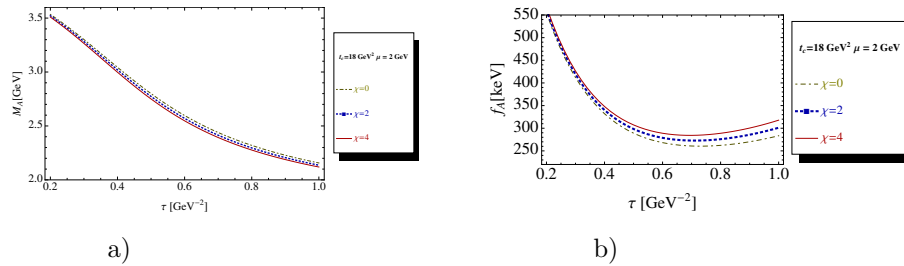


Fig. 66. **a)** M_{A_c} as function of τ , for different values of the $d = 7$ condensate contribution (χ measures the violation of factorization), at a given value of $t_c = 18 \text{ GeV}^2$, $\mu = 2 \text{ GeV}$ and for the QCD parameters in Tables 2 and 3; **b)** The same as a) but for the coupling f_{A_c} .

see a τ -stability of about 0.6 GeV^{-2} starting from $t_c = 12 \text{ GeV}^2$ while t_c -stability is reached from $t_c = 18 \text{ GeV}^2$. At lowest order, one obtains for $\mu = 2 \text{ GeV}$:

$$M_{A_c}^{LO} \simeq (2387 \sim 2401) \text{ MeV} \quad \text{and} \quad f_{A_c}^{LO} \simeq (256 \sim 261) \text{ keV}. \quad (72)$$

- The effect on the choice of mass (running or pole) is shown in Fig. 63.
- The effects of the truncation of the PT series are shown in Fig. 64 where one can notice that the PT corrections are small both for the coupling and for the mass.

- The analysis of the μ -behaviour in Fig. 65 indicates a μ -stability for $\mu = 2$ GeV.
- We show in Fig. 66 the effect of a class of $d = 7$ condensates for different values of the factorization violation parameter χ . Our estimate of the error induced by the truncation of the OPE corresponds to the choice $\chi = 4$.
- From the previous analysis, we deduce the final result including N2LO PT perturbative $\oplus d \leq 6$ dimension contributions:

$$\begin{aligned} M_{A_c} &\simeq (2400 \pm 47) \text{ MeV} , \\ \hat{f}_{A_c} &\simeq (192 \pm 41) \text{ keV} \quad \Longrightarrow \quad f_{A_c} \simeq (260 \pm 55) \text{ keV} , \end{aligned} \quad (73)$$

where we take $t_c \simeq (12 \sim 18) \text{ GeV}^2$ and the optimal choice $\mu=2 \text{ GeV}$. The different sources of errors come from Table 6.

Table 7. Exotic hadron masses and couplings from LSR within stability at N2LO

Nature	J^P	Mass [MeV]	\hat{f}_X [keV]	$f_X(4.5)$ [keV]
b-quark channel				
<i>Molecule</i>				
B^*K	1^+	5186 ± 13	4.48 ± 1.45	8.02 ± 2.60
BK	0^+	5195 ± 15	2.57 ± 0.75	8.26 ± 2.40
$B_s^*\pi$	1^+	5200 ± 18	5.61 ± 0.87	10.23 ± 1.59
$B_s\pi$	0^+	5199 ± 24	3.15 ± 0.70	10.5 ± 2.30
<i>Four-quark</i> $(su)(\bar{b}\bar{d})$				
A_b	1^+	5186 ± 16	5.05 ± 1.32	9.04 ± 2.37
S_b	0^+	5196 ± 17	2.98 ± 0.70	9.99 ± 2.36
c-quark channel				
<i>Molecule</i>				
D^*K	1^+	2395 ± 48	155 ± 36	226 ± 52
DK	0^+	2402 ± 42	139 ± 26	254 ± 48
$D_s^*\pi$	1^+	2395 ± 48	215 ± 35	308 ± 49
$D_s\pi$	0^+	2404 ± 37	160 ± 22	331 ± 46
<i>Four-quark</i> $(su)(\bar{c}\bar{d})$				
A_c	1^+	2400 ± 47	192 ± 41	260 ± 55
S_c	0^+	2395 ± 68	122 ± 26	221 ± 47

18. $X(5568)$ as a four-quark state-molecule mixing

As one can see from Table 7, our predictions do not support the assignments for the $X(5568)$ being a pure BK molecule or four-quark state.^{14, 16–18, 101, 102} Assuming, for instance, that it can result from the mixing of the BK molecule and four-quark state, we consider the two-component mixing:

$$\begin{aligned} |X\rangle &= |B\bar{K}\rangle \cos \theta + |(bu)(\bar{d}\bar{s})\rangle \sin \theta \\ |X_\perp\rangle &= -|B\bar{K}\rangle \sin \theta + |(bu)(\bar{d}\bar{s})\rangle \cos \theta . \end{aligned} \quad (74)$$

Using our result: $M_{BK} \simeq M_{(bu)(\bar{d}\bar{s})} \simeq 5196$ MeV, one can deduce for reproducing $M_X = 5568$ MeV:

$$\sin 2\theta \simeq 0.15, \quad (75)$$

and its orthogonal component: $M_{X_\perp} \simeq 4791$ MeV, which is much below the $\bar{B}K$ threshold. This result may go in line with the one in ¹⁰⁸.

19. Summary and conclusions

- We have studied the masses and couplings of the heavy-light exotic states built from one heavy quark and the three light quarks u,d,s using Laplace sum rule (LSR) within stability (minimum or inflexion point) criteria where N2LO perturbative \oplus dimension $d \leq 6$ condensates contributions have been included.

- Our analysis including higher order PT corrections has given a more meaning on the input value and definition of the heavy quark mass used. We have shown that in this channel the PT corrections are small which (a posteriori) validates the LO \oplus the running mass results often used in the current literature.

- We have compared numerically our QCD expressions with the one in the literature. To our surprise there are disagreement among these though numerically these differences affect only slightly the predictions given by different authors.

- Comparing our predictions with other authors, we found that the existing results are obtained in the region of τ outside the stability region where they are both sensitive to the change of τ (sum rule variable) and of t_c (continuum threshold) which renders the predictions unreliable.

- Our results within stability criteria are summarized in Table 7 where one can notice that, contrary to previous claims,^{14, 16–18, 101–105} we do not predict a mass of a pure exotic BK , B^*K , $B_s\pi$ molecule and/or four-quark $(bu)(\bar{d}\bar{s})$ state around or above the $D0$ candidate $X(5568)$ ¹ which is not confirmed by LHCb.² Our results do not also favour mass values derived from coupled channel analysis and from some other approaches (see e.g.¹⁰⁶ and references quoted therein).

- We have extended the analysis to the charm sector where the results are also summarized in Table 7.

- We notice from Table 7 that the molecule and four-quark state are almost degenerated. The same feature appears for the 0^+ scalar and 1^+ axial-vector states.

- From our analysis, one may suggest experimentalists to scan the regions $(2327 \sim 2444)$ MeV and $(5173 \sim 5226)$ MeV for detecting these unmixed ($cuds$) and ($buds$) exotic hadrons (if any) via eventually their radiative or $\pi + \text{hadrons}$ decays. In the charm sector, the $D_{s0}^*(2317)$ seen by BABAR¹⁰⁷ in the $D_s\pi$ invariant mass, expected to be an isoscalar-scalar state with a width less than 3.8 MeV⁶⁶ could be a good candidate for one of such states.

- If the $X(5568)$ is experimentally confirmed, one can, for instance, interpret it, within our results in Table 7, by a state resulting from a mixing of a BK molecule with a scalar four-quark $(ds)(\bar{b}\bar{u})$ state with a mixing angle: $\sin 2\theta \simeq 0.15$. This result may go in line with the one in ¹⁰⁸.

References

1. V.M. Abazov et al., the $D0$ collaboration, arXiv:1602.07588v2 [hep-ex] (2016).
2. J. van Tilburg, the $LHCb$ collaboration, LHCb-CONF-2016-004, 51ème Rencontre de Moriond, La Thuile, Italy (2016).
3. M.A. Shifman, A.I. Vainshtein and V.I. Zakharov, *Nucl. Phys.* **B147** (1979) 385.
4. M.A. Shifman, A.I. Vainshtein and V.I. Zakharov, *Nucl. Phys.* **B147** (1979) 448.
5. S. Narison, *Nucl. Part. Phys. Proc.* **207-208** (2010) 315.
6. S. Narison, *Nucl. Part. Phys. Proc.* **258-259** (2015) 189.
7. S. Narison, *QCD as a theory of hadrons, Cambridge Monogr. Part. Phys. Nucl. Phys. Cosmol.* **17** (2002) 1 [hep-ph/0205006].
8. S. Narison, *QCD spectral sum rules*, *World Sci. Lect. Notes Phys.* **26** (1989) 1.
9. S. Narison, *Phys. Rept.* **84** (1982) 263.
10. S. Narison, *Acta Phys. Pol.* **B26** (1995) 687.
11. S. Narison, hep-ph/9510270 (1995).
12. L.J. Reinders, H. Rubinstein and S. Yazaki, *Phys. Rept.* **127** (1985) 1.
13. E. de Rafael, hep-ph/9802448.
14. S. S. Agaev, K. Azizi and H. Sundu, arXiv:1603.02708.
15. S. S. Agaev, K. Azizi and H. Sundu, *Phys. Rev.* **D93** (2016) n^o 7, 074024.
16. C.M. Zanetti, M. Nielsen and K.P. Khemchandani, arXiv:1602.09041v1 [hep-ph].
17. W. Chen et al., arXiv:1602.08916v1 [hep-ph].
18. Z.-G. Wang, arXiv:1602.08711v1 [hep-ph].
19. J.S. Bell and R.A. Bertlmann, *Nucl. Phys.* **B227** (1983) 435.
20. R.A. Bertlmann, *Acta Phys. Austriaca* **53** (1981) 305.
21. S. Narison, E. de Rafael, *Phys. Lett.* **B103** (1981) 57.
22. S. Narison, *Phys. Lett.* **B210** (1988) 238.
23. S. Narison, *Phys. Lett.* **B337** (1994) 166.
24. S. Narison, *Phys. Lett.* **B322** (1994) 327.
25. S. Narison, *Phys. Lett.* **B387** (1996) 162.
26. S. Narison, *Phys. Lett.* **B358** (1995) 113.
27. S. Narison, *Phys. Lett.* **B466** (1999) 345.
28. S. Narison, *Phys. Lett.* **B605** (2005) 319.
29. S. Narison, *Phys. Rev.* **D74** (2006) 034013.
30. S. Narison, *Phys. Lett.* **B668** (2008) 308.
31. R.M. Albuquerque, S. Narison, *Phys. Lett.* **B694** (2010) 217.
32. R.M. Albuquerque, S. Narison, M. Nielsen, *Phys. Lett.* **B684** (2010) 236.
33. S. Narison, F. Navarra and M. Nielsen, *Phys. Rev.* **D83** (2011) 016004.
34. S. Narison, *Phys. Lett.* **B718** (2013) 1321.
35. S. Narison, *Nucl. Part. Phys. Proc.* **234** (2013) 187.
36. E. de Rafael, *Nucl. Part. Phys. Proc.* **96** (2001) 316.
37. S. Peris, B. Phily and E. de Rafael, *Phys. Rev. Lett.* **86** (2001) 14.
38. P.M. Stevenson, *Nucl. Phys.* **B868** (2013) 38.
39. K. Chetyrkin, S. Narison and V.I. Zakharov, *Nucl. Phys.* **B550** (1999) 353.
40. S. Narison and V.I. Zakharov, *Phys. Lett.* **B522** (2001) 266.
41. V.I. Zakharov, *Nucl. Phys. Proc. Suppl.*, **164** (2007) 240.
42. S. Narison, *Nucl. Phys. Proc. Suppl.* **164** (2007) 225.
43. S. Narison and V.I. Zakharov, *Phys. Lett.* **B679** (2009) 355.
44. F. Fanomezana, S. Narison and A. Rabemananjara, *Nucl. Part. Phys. Proc.* **258-259** (2015) 152.
45. F. Fanomezana, S. Narison and A. Rabemananjara, *Nucl. Part. Phys. Proc.* **258-259** (2015) 156.

46. A. Pich and E. de Rafael, *Phys. Lett.* **B158** (1985) 477.
47. S. Narison and A. Pivovarov, *Phys. Lett.* **B327**(1994) 341.
48. E.G. Floratos, S. Narison and E. de Rafael, *Nucl. Phys.* **B155** (1979) 155.
49. C. Becchi et al., *Z. Phys.* **C8** (1981) 335.
50. D.J. Broadhurst, *Phys. Lett.* **B101** (1981) 423.
51. K.G. Chetyrkin, J.H. Kühn and M. Steinhauser, *Eur. Phys. J.* **C21** (2001) 319.
52. R. Tarrach, *Nucl. Phys.* **B183** (1981) 384.
53. R. Coquereaux, *Annals of Physics* **125** (1980) 401.
54. P. Binetruy and T. Sücker, *Nucl. Phys.* **B178** (1981) 293.
55. S. Narison, *Phys. Lett.* **B197** (1987) 405.
56. S. Narison, *Phys. Lett.* **B216** (1989) 191.
57. N. Gray et al., *Z. Phys.* **C48** (1990) 673.
58. L.V. Avdeev and M. Yu. Kalmykov, *Nucl. Phys.* **B502** (1997) 419.
59. J. Fleischer et al., *Nucl. Phys.* **B539** (1999) 671.
60. K.G. Chetyrkin and M. Steinhauser, *Nucl. Phys.* **B573** (2000) 617.
61. K. Melnikov and T. van Ritbergen, *Phys. Lett.* **B482** (2000)99.
62. S. Narison, *Phys. Lett.* **B673** (2009) 30.
63. E. Braaten, S. Narison and A. Pich, *Nucl. Phys.* **B373** (1992) 581.
64. S. Narison and A. Pich, *Phys. Lett.* **B211** (1988) 183.
65. For a recent review, see e.g: S. Bethke, *Nucl. Phys. Proc. Suppl.* **234** (2013) 229.
66. K.A. Olive et al. (Particle Data Group), *Chin. Phys.* **C38** (2014) 090001.
67. S. Narison, *Phys. Lett.* **B693** (2010) 559; Erratum ibid 705 (2011) 544.
68. S. Narison, *Phys. Lett.* **B706** (2011) 412.
69. S. Narison, *Phys. Lett.* **B707** (2012) 259.
70. B.L. Ioffe and K.N. Zybalyuk, *Eur. Phys. J.* **C27** (2003) 229.
71. B.L. Ioffe, *Prog. Part. Nucl. Phys.* **56** (2006) 232.
72. H.G. Dosch and S. Narison, *Phys. Lett.* **B417** (1998) 173.
73. S. Narison, *Phys. Lett.* **B216** (1989) 191.
74. S. Narison, *Phys. Lett.* **B738** (2014) 346.
75. Y. Chung et al., *Z. Phys.* **C25** (1984) 151.
76. H.G. Dosch, *Non-Perturbative Methods (Montpellier 1985)* ed. S. Narison, WSC.
77. H.G. Dosch, M. Jamin and S. Narison, *Phys. Lett.* **B220** (1989) 251.
78. B.L. Ioffe, *Nucl. Phys.* **B188** (1981) 317.
79. B.L. Ioffe, *Nucl. Phys.* **B191** (1981) 591.
80. A.A.Ovchinnikov and A.A.Pivovarov, *Yad. Fiz.* **48** (1988) 1135.
81. G. Launer, S. Narison and R. Tarrach, *Z. Phys.* **C26** (1984) 433.
82. S. Narison, *Phys. Lett.* **B300** (1993) 293.
83. S. Narison, *Phys. Lett.* **B361** (1995) 121.
84. F.J. Yndurain, *Phys. Rept.* **320** (1999) 287.
85. R.A. Bertlmann and H. Neufeld, *Z. Phys.* **C27** (1985) 437.
86. S. Narison, *Phys. Lett.* **B361** (1995) 121.
87. S. Narison, *Phys. Lett.* **B624** (2005) 223.
88. S. Narison, *Phys. Lett.* **B387** (1996) 162.
89. A. Pich and A. Rodriguez-Sánchez, arXiv:1605.06830 [hep-ph] (2016).
90. M. Davier et al., *Eur. Phys. J.* **C56** (2008) 305.
91. D. Boito et al, *Phys. Rev.* **D95** (2015) **n**⁰**3**, 034003.
92. D. Boito et al, *Nucl. Part. Phys. Proc.* **270-272** (2016) 103.
93. J. Rosner and S. Stone, arXiv:1509.02220 [hep-ph] (2015).
94. S. Aoki et al., FLAG working group, *Eur. Phys. J.* **C74** (2014) 2890 .
95. G. S. Bali, C. Bauer and A. Pineda, *Phys. Rev. Lett.* **113** (2014) 092001.

96. T. Lee, *Phys. Rev.* **D82**(2010)114021.
97. R.A. Bertlmann, G. Launer and E. de Rafael, *Nucl. Phys.* **B250** (1985) 61.
98. R.A. Bertlmann et al., *Z. Phys.* **C39** (1988) 231.
99. S. Narison, *Int. J. Mod. Phys.* **A30** (2015) n^0 **20**, 1550116.
100. S. Narison, *Nucl. Part. Phys. Proc.* **270-272** (2016) 143.
101. W. Wang and R.-L. Zhu, arXiv: 1602.08806 [hep-ph] (2016).
102. A. Ali et al., arXiv: 1604.01731 [hep-ph] (2016).
103. T.J. Burns and E.S. Swanson, arXiv: 1603.04366 [hep-ph] (2016).
104. F.R. Guo, U.G. Meissner and B.S. Zou, arXiv: 1603.06316 [hep-ph] (2016).
105. X. Chen, J. Ping, arXiv: 1604.05651 [hep-ph] (2016).
106. M. Albaladejo et al., arXiv: 1603.09230 [hep-ph] (2016).
107. B. Aubert et al., *the BABAR collaboration*, *Phys. Rev. Lett.* **90** (2003) 242001.
108. A. Esposito, A. Pilloni and A.D. Polosa, *Phys. Lett.* **B758** (2016) 292.